

Searching for T dwarfs in the ρ Oph dark cloud L 1688

Poshih Chiang,¹★ Wen-Ping Chen,¹ Loïc Albert,² Michael Liu³
and Eugene A. Magnier³

¹Graduate Institute of Astronomy, National Central University, 300 Jhongda Road, Jhongli 32001, Taiwan

²Département de physique and Observatoire du Mont Mégantic, Université de Montréal, CP 6128, Succursale Centre-Ville, Montréal, QC H3C 3J7, Canada

³Institute for Astronomy, University of Hawaii, 2680 Woodlawn Dr., Honolulu, HI 96822, USA

Accepted 2014 December 18. Received 2014 December 12; in original form 2014 June 30

ABSTRACT

We present a list of T dwarf candidates in the dark cloud L 1688 in the ρ Oph star-forming region. These candidates are selected with infrared colours sensitive to T dwarf characteristics of methane absorptions and of cool atmospheres. The 1.6- μm methane feature is diagnosed by on–off imaging using an *H*-band and an intermediate-band methane filter, calibrated to a set of known brown dwarfs of M, L, and T types in the field. Another methane feature at 3.3 μm is traced with the *Spitzer*/Infrared Array Camera (IRAC) [3.6] – [4.5] colour. For cool atmospheres, the *H* – [4.5] and *K* – [4.5] colours are utilized. With an additional criterion of mid-infrared brightness to eliminate extragalactic interlopers, a total of 28 T dwarf candidates have been identified. A comprehensive assessment was conducted to estimate the level of contamination of our sample by young stellar variability, by extragalactic sources sharing the same colour behaviour, or by foreground T dwarfs. Though extragalactic sources may contribute up to about half of the false positives, our candidates show close spatial association with the dark cloud, rather than randomly distributed as a background population would have been. Furthermore, even though our candidates are not selected a priori by a colour–magnitude relation, they mostly follow the 1 Myr isochrones, ascertaining their youth. Our selection methodology provides guidance to search for T dwarfs in other star-forming regions. Our candidate list, when comparing with those in the literature, which often rely on a single criterion on cool temperature or methane, is more conservative but should be more secure for follow-up spectroscopic confirmation of a T dwarf sample at the early evolutionary stage.

Key words: brown dwarfs – stars: pre-main sequence – ISM: individual objects: L1688.

1 INTRODUCTION

Kumar (1963) and Hayashi & Nakano (1963) pioneered the theoretical studies of brown dwarfs, followed by later works of Burrows & Liebert (1993), Burrows et al. (2001), Chabrier & Baraffe (2000), Baraffe et al. (2002), and Baraffe et al. (2003). After the first brown dwarf was discovered (Nakajima et al. 1995; Rebolo, Zapatero Osorio & Martín 1995) more were found by large sky surveys such as 2MASS, DENIS, SDSS, and *WISE* (Kirkpatrick et al. 2011). The spectral classification and observational characteristics of brown dwarfs were reviewed by Basri (2000) and Kirkpatrick (2005). The cool surface temperature of a brown dwarf allows formation of dust and molecules in its atmosphere. In infrared, the presence of dust and molecules sculpts the spectral energy distributions and hence influences on the observational characteristics of

brown dwarfs (Kirkpatrick 2005). For instance, the coolest brown dwarfs feature methane absorptions in their spectra.

To date, some 1200 brown dwarfs (see DwarfArchive¹ for listing) have been discovered. However, their formation mechanism remains controversial. Do brown dwarfs form like stars via circumstellar accretion, and get ejected as a result of dynamical interaction in bound stellar systems or turbulent fragments, or do they, like planets, condense out of circumstellar discs (Whitworth et al. 2007)? To answer questions like these, identification of the youngest and coolest brown dwarfs, i.e. T dwarfs, is an important first step. Younger brown dwarfs are easier to detect, before they cool down and fade out quickly after birth (Burrows et al. 2001; Saumon & Marley 2008). Recent observations to search for young substellar objects in star-forming regions have pushed the detected mass down to the planetary realm, e.g. Béjar et al. (2011) and Peña Ramírez et al. (2012) on σ Orion; Scholz et al. (2012) on NGC1333; Burgess

* E-mail: pschiang@gmail.com

¹ <http://DwarfArchives.org>

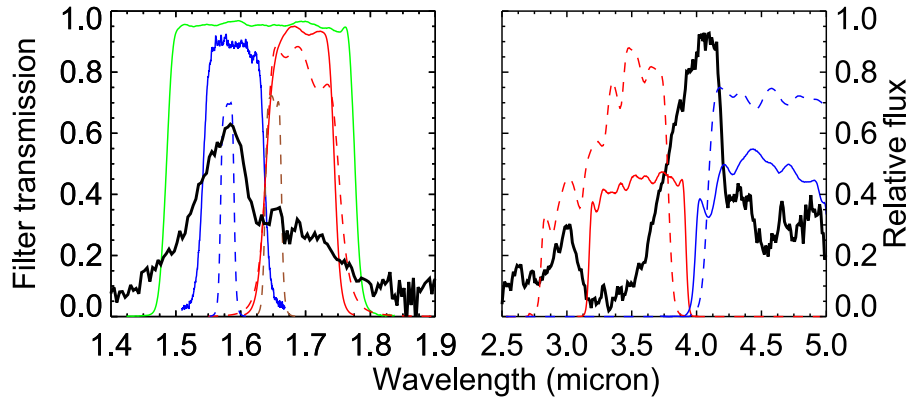


Figure 1. Left: the example spectrum (shown in relative flux as a black line) of 2MASS J10595219+3041498 (in black), a T4 dwarf, shows the suppression near $1.6\ \mu\text{m}$ due to methane absorption. Transmission curves of CFHT H (in green), CH_4OFF (in blue) and CH_4ON (in red) are shown in thin solid lines. Those of Gemini Hcon (in blue), $[\text{Fe II}]$ (in brown), and $\text{CH}_{4\text{long}}$ (in red) are in dashed lines. Right: the example spectrum of a T4.5 dwarf 2MAS J0559–1404 obtained by *Akari* (Sorahana & Yamamura 2012) is shown as a black line. The transmission curves of IRAC and *WISE* are shown in solid and dashed lines, respectively. The shapes of the transmission curves in IRAC Channel 1 (red solid line) and *WISE* W1 (red dashed line) are significantly different, while those in the IRAC Channel 2 (blue solid line) and *WISE* W2 (blue dashed line) are similar.

et al. (2009) on IC348; Luhman (2004b) on Chamaeleon; Luhman (2004a) on Taurus; Comerón, Spezzi & López Martí (2009) on Lupus; Lodieu et al. (2011) on Upper Scorpius; and Spezzi et al. (2012) on Serpen.

The ρ Ophiuchi cloud, at a distance of 130 pc and with an age of ~ 1 Myr (Wilking, Gagné & Allen 2008), is an ideal hunting ground for brown dwarfs. Our study focuses on L 1688, the most active star-forming cloud in the whole ρ Oph complex. The clumpiness of molecular clouds leads to a highly variable extinction ($A_K = 0.5$ to ≥ 4.0) in this region (Chapman et al. 2009). There exists a wealth of data on the young stellar population in the region, but despite hundreds of substellar candidates identified with different methods, such as by fitting the spectral energy distribution of JHK , $3.6\ \mu\text{m}$, to $4.5\ \mu\text{m}$ (Marsh et al. 2010b; Barsony et al. 2012), by JHK two-colour and colour–magnitude diagrams (CMDs; Alves de Oliveira et al. 2010), by iJK two-colour and colour–magnitude diagrams (Geers et al. 2011), or by methane on–off imaging (Haisch, Barsony & Tinney 2010), most of the confirmed candidates are late-M or L dwarfs, with only one early-T claimed by Marsh, Kirkpatrick & Plavchan (2010a).

In this work, we select T dwarf candidates with broad-band colours and with methane absorptions at 1.6 and $3.3\ \mu\text{m}$, based on the criteria defined by confirmed field brown dwarfs. In Section 2, we demonstrate how the selection parameters are determined empirically from known M, L, and T dwarfs, and in Section 3 how these parameters are used to search for T dwarfs in L 1688. In Section 4, we consider possible contamination, Galactic, or extragalactic, in our sample. In Section 5, we compare our candidate list with those previously published, and discuss the implication of the young T dwarf population. The results of our study are summarized in Section 6.

2 CHARACTERIZATION OF FIELD T DWARFS

T dwarfs are characterized by cool atmospheres and by methane absorptions in their spectra. Methane absorptions near 1.6 and $3.3\ \mu\text{m}$ can be diagnosed either by customized filters at $1.6\ \mu\text{m}$ (Rosenthal, Gurwell & Ho 1996; Tinney et al. 2005), by *WISE* colour $W1 - W2$ (hereafter $[3.4] - [4.6]$) (Kirkpatrick et al. 2011), or by *Spitzer*/Infrared Array Camera (IRAC) IRAC1 – IRAC2 (hereafter $[3.6] - [4.5]$) (Patten et al. 2006). On the other hand, colour indices

$K - [4.5]$ and $H - [4.5]$ serve as temperature and spectral type indicators, respectively (Patten et al. 2006; Leggett et al. 2010). In our analysis, we determined the empirical infrared colour distributions of T dwarfs on the basis of a sample of spectroscopically confirmed M, L, and T dwarfs. These relations, in turn, were used to identify T dwarf candidates in ρ Oph.

2.1 CFHT/WIRCam observations

To examine the methane absorption near $1.6\ \mu\text{m}$, a snapshot programme was carried out with the Wide-field Infrared Camera (WIRCam) on the 3.6 m Canada–France–Hawaii Telescope (CFHT) in 2010. The WIRCam is composed of 2×2 HAWAII-2RG infrared detectors, each of which consists of 2048×2048 pixels with 0.3 arc-sec pixel^{-1} on the sky, rendering a field of view about 20 arcmin $\times 20$ arcmin. In addition to the standard JHK filters, WIRCam equips with a pair of methane filters CH_4ON and CH_4OFF . The CH_4ON filter is centred on the methane absorption at $1.6\ \mu\text{m}$ with a bandwidth of $0.1\ \mu\text{m}$. The CH_4OFF , centred at $1.58\ \mu\text{m}$, is used to estimate the pseudo-continuum. However, the CH_4OFF filter was unavailable during our WIRCam run in 2010, so instead, a broad-band H filter was used. Fig. 1 shows the transmission curves of CFHT/WIRCam CH_4OFF , H , CH_4ON , and Gemini/NIRI Hcon, $[\text{Fe II}]$, $\text{CH}_{4\text{long}}$, along with the spectrum of a T4 dwarf (Sheppard & Cushing 2009). The differential fluxes between CH_4ON and the continuum (CH_4OFF or H) are used to identify possible $1.6\text{-}\mu\text{m}$ methane absorption.

Observations in H and CH_4ON were obtained in Queue Service Observing between 2010 March 28 and April 24 for 28 L and T dwarfs (see Table 1) selected from the DwarfArchive catalogue. The 7.5-s integrations per filter and target consisted in individual 2.5-s correlated double-sampled exposures on a three-point dither pattern.

Raw data were processed at CFHT using the *IWI* pipeline² which applies reference pixel correction, non-linearity correction, dark subtraction, bad pixel masking, flat fielding using dome flats, amplifier cross-talk correction, and sky subtraction. It also provides

² <http://www.cfht.hawaii.edu/Instruments/Imaging/WIRCam/IwiVersion1-Doc.html>

Table 1. Known L and T dwarfs in the CFHT/WIRCam snapshot programme.

Spectral type	RA(J2000) (deg)	Dec(J2000) (deg)	2MASS <i>H</i> (mag)	CFHT <i>H</i> (mag)	CFHT CH ₄ ON (mag)	Name
L1	220.067 5324	0.444 2094	15.41 (0.12)	15.30 (0.03)	15.21 (0.04)	SDSS J144016.20+002638.9
L1	187.688 5205	28.466 0064	15.00 (0.08)	15.07 (0.01)	14.87 (0.04)	2MASS J12304562+2827583
L3	168.333 8914	34.516 2220	15.80 (0.20)	15.99 (0.06)	15.60 (0.10)	SDSS J111320.16+343057.9
L4	209.301 7041	14.477 8439	14.65 (0.06)	14.58 (0.01)	14.41 (0.02)	SDSS J135712.40+142839.8
L5.5	201.623 3829	-0.642 3062	15.05 (0.06)	15.06 (0.02)	14.90 (0.04)	SDSSp J132629.82-003831.5
L5.5	205.512 8859	13.672 7806	15.71 (0.11)	15.87 (0.06)	15.80 (0.07)	SDSS J134203.11+134022.2
L6	158.341 6056	40.096 5875	15.87 (0.18)	16.16 (0.08)	16.22 (0.13)	SDSS J103321.92+400549.5
L7	161.039 0883	4.494 2006	14.95 (0.07)	15.07 (0.02)	14.99 (0.03)	SDSS J104409.43+042937.6
L7.5	178.973 2042	5.999 2187	14.70 (0.07)	14.72 (0.03)	14.52 (0.04)	SDSS J115553.86+055957.5
L8	151.798 3983	19.515 7078	15.76 (0.15)	15.75 (0.04)	15.54 (0.06)	SDSS J100711.74+193056.2
L9.5	157.611 7208	2.218 6854	16.18 (0.19)	16.26 (0.06)	16.05 (0.07)	SDSS J103026.78+021306.4
T0	181.945 0731	2.740 6688	14.56 (0.07)	14.63 (0.01)	14.53 (0.01)	SDSS J120747.17+024424.8
T1	159.880 5579	32.940 28170	15.34 (0.11)	15.42 (0.04)	15.40 (0.08)	SDSS J103931.35+325625.5
T1.5	210.731 9570	8.015 0559	15.97 (0.16)	16.20 (0.08)	16.20 (0.11)	SDSS J140255.66+080055.2
T2.5	162.121 0966	9.327 7941	15.90 (0.16)	16.04 (0.08)	16.13 (0.12)	SDSS J104829.21+091937.8
T2.5	211.207 0381	-31.992 4001	14.96 (0.07)	14.85 (0.07)	14.95 (0.09)	2MASS J14044948-3159330
T3	155.289 8308	-3.072 3321	15.35 (0.10)	15.55 (0.05)	15.78 (0.08)	SDSS J102109.69-030420.1
T3	182.484 6385	-10.067 9666	15.33 (0.09)	15.25 (0.02)	15.26 (0.04)	2MASS J12095613-1004008
T3	213.875 3056	57.407 3840	15.82 (999)	16.09 (0.11)	15.97 (0.14)	SDSS J141530.05+572428.7
T4	164.965 0510	30.700 0960	15.77 (0.12)	15.90 (0.05)	16.03 (0.10)	2MASS J10595185+3042059
T4.5	209.719 4378	37.785 9427	16.14 (0.17)	16.31 (0.08)	16.69 (0.17)	SDSS J135852.68+374711.9
T5.5	167.540 9837	1.269 5891	15.92 (0.14)	16.10 (0.08)	16.96 (0.31)	SDSSp J111010.01+011613.1
T5.5	187.944 6588	8.789 7329	15.31 (0.11)	15.51 (0.05)	15.91 (0.18)	2MASS J12314753+0847331
T6	186.477 5527	-27.664 8756	15.10 (0.08)	15.05 (0.06)	15.51 (0.13)	2MASS J12255432-2739466
T6.5	161.968 1370	21.405 0034	15.80 (0.12)	15.83 (0.05)	16.07 (0.13)	2MASS J1047538+212423
T6.5	206.691 8690	-0.530 8726	15.47 (0.12)	15.87 (0.06)	16.56 (0.23)	SDSSp J134646.45-003150.4
T7.5	184.292 7785	-3.186 7238	15.75 (0.12)	16.07 (0.06)	16.86 (0.17)	2MASS J1217110-031113
T7.5	224.315 8458	-21.368 7564	15.27 (0.09)	15.27 (0.05)	16.17 (0.14)	Gliese 570D

a photometric calibration for each detector (no colour correction) and a rough linear astrometry solution, both using 2MASS stars.

Fine astrometric calibrations were done with SCAMP and the images were co-added with SWARP³ (Bertin et al. 2002). Aperture photometry was performed with the IRAF package APPHOT. The *H*-band instrumental magnitudes of all objects, including field stars and brown dwarfs, were calibrated to 2MASS *H*. Under the assumption that most field stars have no methane absorption, we scaled the CH₄ON instrumental magnitudes to the calibrated *H* magnitudes.

We defined the magnitude difference $R_{1.6} = \text{mag}_H - \text{mag}_{\text{CH}_4\text{ON}}$ as a measure of the strength of the methane absorption at 1.6 μm ; that is, an object with a methane absorption would have a negative $R_{1.6}$ value.

2.2 Synthetic photometry of known brown dwarfs

Our snapshot programme provides directly the observed $R_{1.6}$ values. In addition, to compute how the $R_{1.6}$ index varies with a wide spectral range, we converted the infrared spectra of M, L, and T dwarfs available in Spex Prism Spectral Libraries⁴ into magnitudes by convolving with the transmission curves of filters. The synthetic magnitude is derived by

$$\text{mag}_{\text{syn}} = \frac{\int \lambda F(\lambda) S(\lambda) d\lambda}{\int \lambda S(\lambda) d\lambda}, \quad (1)$$

where $F(\lambda)$ is the stellar spectra, and $S(\lambda)$ is the transmission curve of a particular filter. Only the differences of magnitudes, i.e. colours,

³ <http://www.astromatic.net/software/swarp>

⁴ <http://pono.ucsd.edu/~adam/browndwarfs/spexprism/>

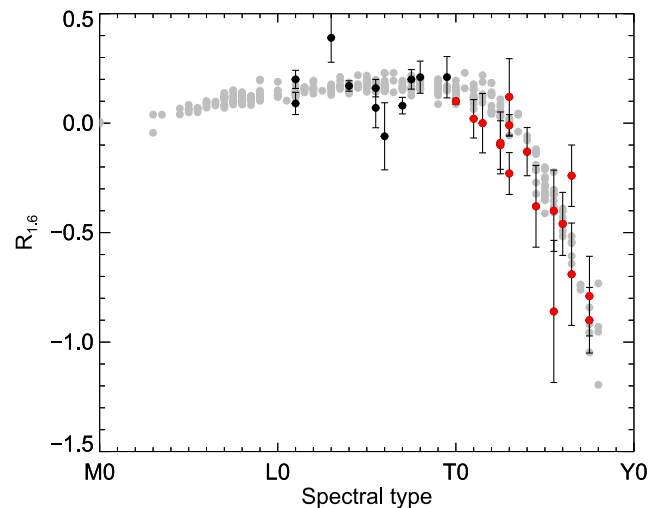


Figure 2. The $R_{1.6} = \text{mag}_H - \text{mag}_{\text{CH}_4\text{ON}}$ index versus spectral type of known M, L, and T dwarfs. Targets observed by the CFHT/WIRCam are marked as black (L dwarfs) and red (T dwarfs) filled circles with errors, whereas those computed from the SpeX library are shown in grey filled circles.

are needed in our analysis, so no corrections of zero magnitudes are necessary.

With the assumption of $R_{1.6} = 0$ for the earliest M dwarfs, we derived the synthetic $R_{1.6}$ index from M to T spectral types, as shown in Fig. 2. It is seen that the synthetic $R_{1.6}$ colours are generally

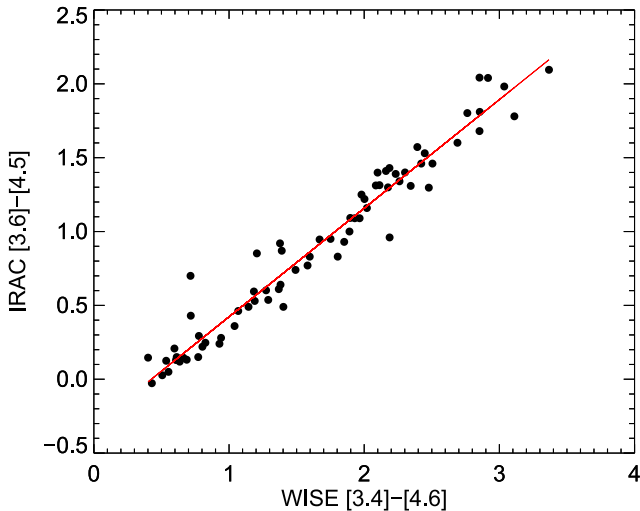


Figure 3. IRAC [3.6] – [4.5] versus WISE [3.4] – [4.6] for T dwarfs. The data were collected for the 72 T dwarfs with good photometric measurements from Patten et al. (2006, their table 3), Leggett et al. (2010, their table 3), Kirkpatrick et al. (2011, their table 1), and Mace et al. (2013, their table 1–3). The line represents the linear regression of the data, namely, $[3.6] - [4.5] = 0.74([3.4] - [4.6]) - 0.31$ used to convert the WISE [3.4] – [4.6] to the IRAC [3.6] – [4.5].

consistent with the observations, with the $R_{1,6}$ index showing a clear drop after the mid-T type, as expected for the increasing methane absorption. To minimize confusion, we set $R_{1,6} < -0.1$, i.e. later than T3/T4, as the threshold to identify T dwarfs.

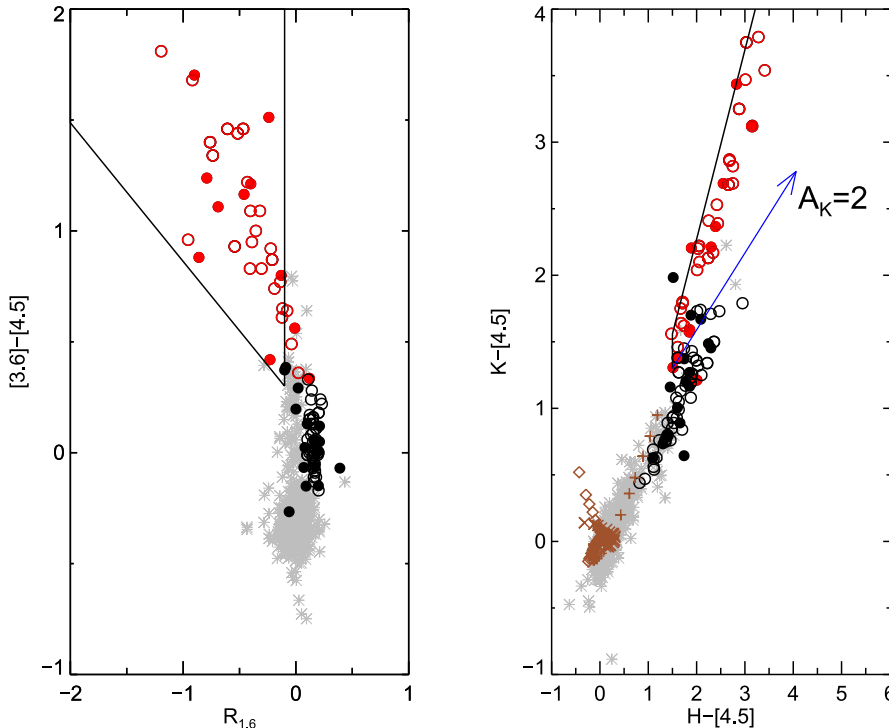


Figure 4. Left: two methane indices of $R_{1,6}$ and $[3.6] - [4.5]$. The WISE [3.4] – [4.6] is transformed to IRAC [3.6] – [4.5] for objects not observed by IRAC (see text). Right: $H - [4.5]$ versus $K - [4.5]$ two-colour diagram. Filled symbols represent our snapshot L dwarfs (black) and T dwarfs (red). Open circles mark additional M/L (black) and T dwarfs (red) listed by Patten and Leggett, for which the $R_{1,6}$ values are synthesized from the Spex library. The region confined by the solid lines in the methane diagram is the empirical T zone separating T dwarfs from field population (grey). Likewise, the T dwarf locus (solid line) is steeper than field population (grey) in the $K - [4.5]$ versus $H - [4.5]$ diagram. Brown symbols represent dwarfs (pluses), giants (crosses), and supergiants (open diamonds) (Ducati et al. 2001). The reddening of $A_K = 2$ is shown by the arrow.

2.2.1 Spitzer and WISE data

We used the snapshot sample, i.e. the spectroscopically confirmed brown dwarfs, to establish the selection criteria with IRAC colours. However, only 10 of our snapshot targets were observed by IRAC (Patten et al. 2006; Leggett et al. 2010), so we converted the WISE colour $[3.4] - [4.6]$ to the IRAC colour $[3.6] - [4.5]$. The transmission curves of $[4.6]$ (W2) and $[4.5]$ (IRAC2) are similar, so $H - [4.6]$ and $K - [4.6]$ serve as $H - [4.5]$ and $K - [4.5]$. Despite the different transmission curves of $[3.4]$ (W1) and $[3.6]$ (IRAC1), the colours $[3.4] - [4.6]$ and $[3.6] - [4.5]$ are linearly correlated for known brown dwarfs, as illustrated in Fig. 3. For the snapshot targets without IRAC observations, their IRAC $[3.6] - [4.5]$ colours therefore were converted from the WISE $[3.4] - [4.6]$ colours.

2.2.2 Empirical colours of T dwarfs

We make use of two kinds of colour–colour diagrams to distinguish T dwarfs, one for the methane absorption features ($[3.6] - [4.5]$ versus $R_{1,6}$), and the other for the cool atmospheres ($K - [4.5]$ versus $H - [4.5]$). Fig. 4 shows such two colour–colour diagrams for known M, L, and T dwarfs. In addition to our snapshot L and T dwarfs, the M/L and T dwarfs listed by Patten et al. (2006) and by Leggett et al. (2010) are also included to define the empirical colours. For the sample in Patten et al. (2006) and in Leggett et al. (2010), their $R_{1,6}$ values are synthesized from the Spex library.

In the methane colour–colour diagram, there is a clear segregation of T dwarfs from field stars and from early M/L types. For T dwarfs, the two methane indices $R_{1,6}$ and $[3.6] - [4.5]$ are positively

Table 2. Observation log of the CFHT/WIRCam data in L 1688.

Run ID	Name	RA(J2000) (deg)	Dec(J2000) (deg)	Exposure time dither \times exposure \times co-add (s)	
2006AF01	RhoOphA	246.792 39	-24.432 66	H:7 \times 7 \times 8, K:7 \times 7 \times 8	2006 Apr 19
2006AF01	RhoOphB	246.457 28	-24.435 24	H:9 \times 7 \times 8, K:11 \times 7 \times 8	2006 Apr 20 2006 May 10
2006AF01	RhoOphC	246.791 66	-24.733 33	H:7 \times 7 \times 8, K:7 \times 7 \times 8	2006 May 9–11
2006AF01	RhoOphD	246.121 32	-24.732 59	H:10 \times 7 \times 8, K:7 \times 7 \times 8	2006 May 11, 19 2006 Jul 7
2006AF01	RhoOphE	246.458 33	-24.133 34	H:7 \times 7 \times 8, K:8 \times 7 \times 8	2006 May 12
2006AF01	RhoOphF	246.791 06	-24.132 44	H:7 \times 7 \times 8, K:7 \times 7 \times 8	2006 May 17
2006AF01	RhoOphG	247.120 47	-24.433 17	H:7 \times 7 \times 8, K:7 \times 7 \times 8	2006 Jul 11–17
2006AF01	RhoOphH	247.120 83	-24.133 341	H:7 \times 7 \times 8, K:7 \times 7 \times 8	2006 Aug 30
2006AF01	RhoOphI	246.458 32	-24.733 341	H:7 \times 7 \times 8, K:7 \times 7 \times 8	2006 Aug 31
2010BT07	Oph-A	246.957 07	-24.433 89	51 \times 48 \times 3	2010 Aug 10, 12, 28, 29
2010BT07	Oph-B	246.619 12	-24.434 91	47 \times 48 \times 3	2010 Aug 12, 29, 30 2010 Sep 24
2010BT07	Oph-C	246.626 11	-24.737 43	52 \times 48 \times 3	2010 Aug 15 2010 Sep 18, 24
2010BT07	Oph-D	246.967 86	-24.738 30	49 \times 48 \times 3	2010 Aug 19 2010 Sep 19, 24, 25
2010BT07	Oph-E	247.044 63	-24.126 90	51 \times 48 \times 3	2010 Aug 19 2010 Sep 20, 21, 22
2010BT07	Oph-F	246.710 88	-24.128 76	61 \times 48 \times 3	2010 Aug 21, 22, 23, 24 2010 Sep 26, 27, 29
2010BT07	Oph-G	247.292 47	-24.434 70	23 \times 48 \times 3	2010 Aug 24 2010 Sep 30

correlated, with larger scattering towards later spectral types. We therefore adopt the threshold $R_{1.6} = -0.1$ and $[3.6] - [4.5] = 0.3$, corresponding roughly to a T3 type, to define the ‘T zone’ as our selection boundary. Such a choice minimizes confusion from field stars, and favours identification of mid- to late-T dwarfs. Likewise, in the $H - [4.5]$ versus $K - [4.5]$ diagram, the T dwarfs trace out a locus distinct from those of field stars and M/L dwarfs. A T zone can hence be prescribed by shifting the T locus along the interstellar reddening vector.

Objects located in the methane T zone are called ‘methane-selected’ sources, and those redder than the T dwarf locus in the $H - [4.5]$ and $K - [4.5]$ two-colour diagram are called ‘temperature-selected’ sources. An object located in both methane and temperature T zones would be identified as a T dwarf candidate. Among the 979 stars observed in the snapshot fields, 53 pass the $R_{1.6} < -0.1$ selection, 19 have $[3.6] - [4.5]$ colours similar to T dwarfs, but none, except known T dwarfs later than T3, satisfy both criteria. Obviously, using two methane indices is much more reliable than with any single index alone.

Even though stellar objects are mostly ruled out from the temperature T zone, contamination by galaxies is possible. In our snapshot fields, all with short exposures, there are three known galaxies, classified by SDSS with their extended morphology, in the temperature T zone. These galaxies are too luminous in mid-infrared wavelengths to be T dwarfs. The contamination by galaxies would become higher in deeper observations such as those towards ρ Oph. Additional constraints to remove contamination will be discussed in Section 4.

Our methane imaging of 28 known L/T dwarfs in the field allows us to quantify the 1.6 μm absorption with respect to the spectral type. Together with the $[3.6] - [4.5]$ colour to detect the 3.3 μm feature, brown dwarfs after the mid-T type can be identified. The $K - [4.5]$ and $H - [4.5]$ colours serve to further constrain the selection criteria

to exclude earlier spectral type objects. These empirical criteria based on methane absorptions and cool temperature are applied to identify possible T dwarfs in the ρ Oph star-forming region.

3 SEARCHING FOR YOUNG T DWARFS IN ρ OPH STAR-FORMING REGION

3.1 Observations and data reduction

We used seven pointings to mosaic an $\sim 0.8 \text{ deg}^2$ area centring on the dark cloud L1688 A deep methane on/off imaging survey was planned using the CH₄ON and CH₄OFF filters on the CFHT/WIRCam. However, we were informed that the CH₄OFF filter would be unavailable in 2010B. In the end, we decided to use the CH₄ON filter alone. The time for CH₄OFF was devoted to CH₄ON observations of Oph-A to Oph-F. Therefore, the effective exposure time of Oph-A to Oph-F were ~ 2 h and of Oph-G was ~ 1 h. Observations were obtained in the first-half nights in August and September, for which the airmass was ~ 1.5 and the typical seeing was 0.7–0.9 arcsec measured from calibrated images. Without CH₄OFF, we used instead archival CFHT/WIRCam broad-band *JHK* data observed in 2006 which Alves de Oliveira et al. (2010) used to search for brown dwarfs. Detail observational information could be found in Alves de Oliveira et al. (2010). Table 2 shows the log of our and archival WIRCam observations.

Raw data were detrended and co-added with the SIMPLE pipeline⁵ (Wang et al. 2010) optimized to reduce WIRCam images. First of all, the SIMPLE pipeline split and processed images by chips. To minimize the influence from sky variation, we grouped dithering frames

⁵ The pipeline is developed by Wei-Hao Wang, with the IDL code available <http://www.asiaa.sinica.edu.tw/~whwang/idl/SIMPLE/>.

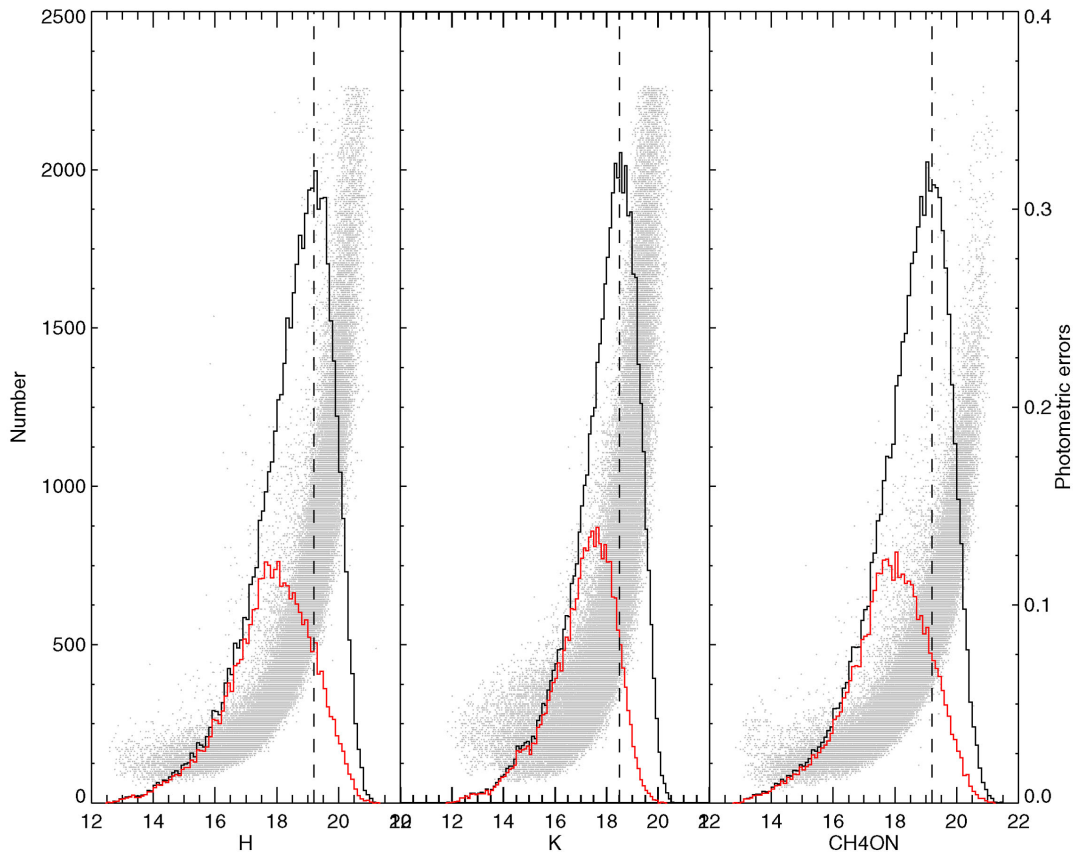


Figure 5. WIRCам photometry in the H , K , and CH_4ON bands. In each panel the apparent magnitude distribution, shown with the left vertical axis, of the entire WIRCам sample is depicted as a black curve, with a dashed line marking the peak. Each red curve represents the apparent magnitude distribution after merging with the c2d catalogue. The photometric uncertainty, with the vertical axis on the right, for each WIRCам source is shown as a grey dot.

every 0.5 h. For dithering frames in the same group, a raw sky flat was determined by the median of dithering frames. Raw images were flattened by the raw flat. Objects were detected and masked in the flattened images. After masking objects, the second sky flat was derived with the median combination and was applied to the final flat correction. After the flat correction, objects in each dither frame were extracted by SExtractor. The positions of objects among different frames were used to calculate and to correct for optical distortion. Sky values were estimated with the flat corrected images and were subtracted from each exposure. After detrending, the astrometric and flux calibrations of archival H and K images in 2006 were solved with the 2MASS catalogue. For the CH_4ON images taken in 2010, we used the H -band source catalogue derived from the 2006 data to do astrometric and flux calibrations. The root mean square of astrometric solution was 0.12–0.15 arcsec for each field. In the end, SIMPLE combined all dithering frames for each pointing. Limited by the array size of IDL, however, SIMPLE could not combine all pointings to produce the final mosaic. Therefore, the final mosaic images are made with the SWARP⁶ software (Bertin et al. 2002). The calibrated WIRCам H magnitudes are used to calibrate the CH_4ON magnitudes, as in the case of the snapshot programme described in the previous section. Photometry is done with the IRAF/DAOPHOT psf photometry package. After astrometric and flux calibrations, we cross-matched detections in H , K , and CH_4ON images within a 1 arcsec radius. Only sources detected in all images were consid-

ered reliable. Finally, we catalogued 53 261 sources in the WIRCам data. Fig. 5 shows the corresponding apparent magnitude distributions and the photometric errors. The 7σ sensitivity limits of H and K were ~ 19.2 and ~ 18.5 mag, respectively, consistent with the Alves de Oliveira et al. (2010) results. The CH_4ON data of Oph-G and of other fields are 0.3 and 0.5 mag deeper than the H -band data at similar photometric errors.

In addition to the near-infrared observations, we also made use of the *Spitzer* c2d mid-infrared photometry to aid our selection. The limiting magnitudes of c2d were [3.6] = 18.0, [4.5] = 17.4, [5.8] = 15.6, [8.0] = 14.2, and [24] = 10. (Evans et al. 2007). Only sources with a quality flag better than ‘D’ (Evans et al. 2007) in IRAC channel 2 (4.5 μm) were included in the analysis. There are 23 974 counterparts, within a 1-arcsec matching radius, between the c2d and our WIRCам catalogues. This merged catalogue serves as the input sample in our analysis, and has apparent magnitude distributions turning over around 17 mag in the WIRCам catalogue, mainly limited by the c2d detection, as seen in Fig. 5, so should have sufficient sensitivity to detect an ~ 900 K T dwarf in ρ Oph, according to the models of Burrows et al. (2001). The WIRCам sources without c2d counterparts should be predominantly background stars.

3.2 T dwarf candidates in ρ Oph

There are noted differences in application of the selection criteria developed from known T dwarfs to ρ Oph. First, sources in ρ Oph would be fainter so photometrically noisier, and suffer more

⁶ www.astromatic.net/software/swarp

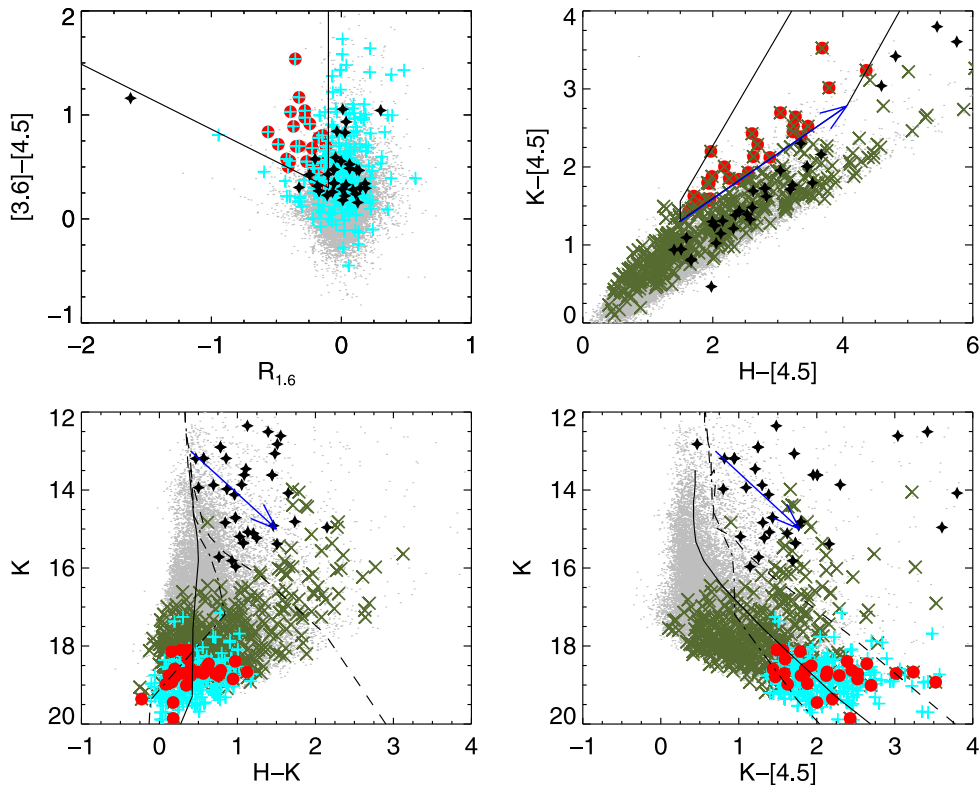


Figure 6. Top: colour–colour diagrams of methane indices (left) and of temperature/spectral type indices (right). The region within which T dwarfs are identified (the T zones) in each diagram is the same as in Fig. 4. The 23 974 WIRCam/c2d sources are represented as grey dots. The methane-selected candidates (441) are marked as green crosses, whereas the temperature-selected candidates (268) as cyan pluses. The T dwarf candidates are represented as filled red circles. Also shown as filled asterisks are the spectroscopically confirmed late-M and L dwarfs in ρ Oph (Alves de Oliveira et al. 2010; Geers et al. 2011; Alves de Oliveira et al. 2012; Mužić et al. 2012). Bottom: the CMDs, with the same symbols as above. The 1 Myr isochrones by the COND (solid line; Baraffe et al. 2003), DUSTY (dashed line; Chabrier & Baraffe 2000), and BT-Settl (dot–dashed line; Allard et al. 2012) models are overlaid. The reddening vectors of $A_{K_s} = 2$ are shown by blue arrows.

extinction than known T dwarfs in the field. Secondly, our observations of ρ Oph were taken with longer exposures, and towards a crowded region of the Milky Way, so contamination is expectedly higher.

Fig. 6 shows the diagnostic colour–colour diagrams in ρ Oph L 1688. The upper panel plots the methane and temperature colour–colour diagrams, together with the empirical T zones, as in Fig. 4 except that here a reddening of $A_K = 2$ appropriate for ρ Oph is applied using the reddening by Chapman et al. (2009). To secure reliability against photometric errors, only candidates with $|R_{1,6}| > \sqrt{\text{err}_{\text{CH}_4\text{ON}}^2 + \text{err}_H^2}$ are considered.

To illustrate how the two diagrams complement each other, and for display clarity, the candidates identified in one diagram are marked separately in the other; that is, those located inside the methane T zone are marked in the temperature diagram, and vice versa. There are a total of 441 methane-selected candidates, and 268 temperature-selected candidates. By combining both selection criteria, the number reduces to 34 as the preliminary T dwarf candidates.

The lower panel of Fig. 6 shows the CMDs to characterize the candidates. The temperature-selected candidates (depicted as cyan pluses) are generally faint ($K > 18$ mag), with $H - K \sim 0-1$, and very red in $K - [4.5]$. In contrast, the methane-selected candidates (green crosses) have a wide range in brightness, with the bright ($K < 17$ mag) ones very red in both $H - K$ and $K - [4.5]$, and

the faint ($K > 18$ mag) sources having $H - K$ colours similar to the temperature candidates with diverse $K - [4.5]$ colours. We interpret the phenomena with the following reasoning.

Galactic dwarfs, giants, or supergiants are ruled out, as demonstrated in Fig. 4, by the temperature T zone. The lack of red objects ($H - K > 1$) is the consequence of the H -band sensitivity. Extragalactic sources, typically red in $K - [4.5]$, predominate the contaminant sample. On the other hand, the methane T zone may be populated by either Galactic or extragalactic sources. Bright methane candidates are likely young stellar objects whose photometric variability leads to false positives in $R_{1,6}$, which was derived from data taken at different epochs. Moreover, the characteristic infrared excess of young stars gives rise to the red $H - K$ and $K - [4.5]$ colours. For faint methane sources, the photometric uncertainties should be responsible for the false $R_{1,6}$ detection and the diversified $K - [4.5]$ colours.

In order to remove galaxies, which are bright in mid-infrared wavelengths, we impose the final condition, namely no detection by *Spitzer*/MIPS, i.e. with a quality flag ‘U’ (Evans et al. 2007). Six candidates are further excluded accordingly. According to the classification in c2d catalogue, two of the six rejected candidates were classified as galaxies, two were red objects, one was cup-down, and one was detected only in [4.5] and [24]. Except one with 7.8 mag, the rest sources range between 9.0 and 9.8 mag in [24]. Comparing with their H -band magnitudes of 18.3–19, these rejected candidates were about 20 times brighter in $24\mu\text{m}$ than in the

Table 3. T dwarf candidates in the ρ Oph.

ID	RA(J2000) (deg)	Dec(J2000) (deg)	H (mag)	$H - K$ (mag)	$R_{1.6}$ (mag)	[4.5] (mag)	[3.6] - [4.5] (mag)	$(\mu_\alpha \cos \delta, \mu_\delta)$ (mas 4yr ⁻¹)	$A_{K_s}^a$ (mag)	Note ^b
1	247.041 831	-24.820 063	19.09 (0.11)	0.16 (0.18)	-0.37 (0.15)	15.403 (0.11)	0.89 (0.15)	(30.1±105.7, -50.0±108.9)	0.75	PM, CH ₄
2	247.059 131	-24.848 191	19.09 (0.11)	0.63 (0.14)	-0.17 (0.13)	15.814 (0.12)	0.38 (0.15)	(33.3±138.3, -63.4±143.2)	0.48	PM
3	246.909 210	-24.877 751	18.38 (0.06)	0.28 (0.09)	-0.13 (0.08)	16.618 (0.13)	0.34 (0.17)	(38.2±84.6, -23.4±84.9)	0.63	PM
4	246.875 510	-24.823 519	19.08 (0.10)	0.11 (0.18)	-0.20 (0.14)	17.086 (0.34)	0.36 (0.44)	(34.0±137.2, 18.0±113.3)	0.73	PM, multi
5	246.615 063	-24.805 047	18.70 (0.11)	0.37 (0.22)	-0.17 (0.17)	16.743 (0.23)	0.40 (0.28)	(-27.5±130.8, -3.6±135.1)	0.42	galaxy?
6	246.783 876	-24.722 407	19.27 (0.12)	0.56 (0.16)	-0.39 (0.16)	16.860 (0.25)	1.03 (0.44)	(-118.4±138.4, -34.9±177.6)	1.57	PM, CH ₄
7	246.803 341	-24.831 998	19.16 (0.14)	0.40 (0.18)	-0.22 (0.17)	16.470 (0.16)	0.48 (0.21)	(-80.0±139.4, 74.2±175.3)	0.62	PM
8	246.666 434	-24.682 725	19.79 (0.17)	0.94 (0.26)	-0.28 (0.22)	16.322 (0.15)	0.97 (0.30)	(-202.2±210.6, 49.7±166.3)	1.44	
9	246.662 498	-24.674 830	20.03 (0.16)	0.18 (0.27)	-0.49 (0.25)	17.428 (0.31)	0.72 (0.79)	(-333.0±171.3, 86.0±165.8)	1.44	
10	246.793 713	-24.887 165	18.98 (0.14)	0.40 (0.20)	-0.35 (0.18)	16.731 (0.19)	0.70 (0.78)	(-62.4±155.7, -23.0±130.8)	0.37	galaxy?
11	246.943 638	-24.827 289	19.43 (0.13)	0.72 (0.17)	-0.40 (0.19)	16.184 (0.14)	0.56 (0.19)	(-247.3±196.2, 131.4±141.2)	0.77	CH ₄
12	246.511 313	-24.764 103	19.41 (0.16)	0.79 (0.22)	-0.21 (0.18)	16.175 (0.16)	0.49 (0.23)	(-246.8±105.7, 212.0±128.2)	0.69	multi
13	246.446 655	-24.638 198	19.51 (0.14)	0.75 (0.18)	-0.24 (0.19)	16.637 (0.27)	0.91 (0.54)	(50.4±159.8, 87.5±160.3)	0.63	PM
14	246.444 858	-24.626 109	18.48 (0.07)	0.37 (0.11)	-0.12 (0.09)	16.540 (0.30)	0.70 (0.67)	(-23.6±89.8, 14.0±97.3)	0.71	PM
15	246.460 843	-24.621 062	18.30 (0.06)	0.16 (0.20)	-0.15 (0.08)	16.355 (0.27)	0.80 (0.43)	(-19.6±77.5, -28.44±88.7)	0.82	PM
16	247.138 864	-24.580 446	18.78 (0.07)	0.20 (0.14)	-0.42 (0.11)	17.150 (0.27)	0.58 (0.39)	(-35.7±136.3, 28.8±121.7)	1.38	PM, CH ₄
17	246.688 499	-24.330 328	19.16 (0.15)	0.49 (0.17)	-0.41 (0.17)	16.533 (0.22)	0.50 (0.30)	(-114.5±132.2, -126.7±109.7)	1.77	multi, CH ₄
17b	246.688 31	-24.330 614	18.8 (0.10)	0.71 (0.13)	-0.3 (0.13)			(32.2±119.3, 1.1±103.0)	1.77	
18	247.123 892	-24.091 061	19.35 (0.14)	0.34 (0.24)	-0.23 (0.18)	16.311 (0.12)	0.68 (0.18)	(-50.3±170.4, 33.5±144.6)	0.73	PM, CH ₄
19	247.167 056	-24.004 751	19.06 (0.11)	0.08 (0.21)	-0.22 (0.14)	17.357 (0.35)	0.52 (0.44)	(13.5±128.2, -97.9±113.9)	0.55	multi
20	247.078 296	-24.134 955	18.88 (0.11)	0.12 (0.24)	-0.18 (0.14)	16.958 (0.26)	0.37 (0.32)	(26.3±103.9, 8.3±109.0)	0.82	PM, multi
20b	247.078 58	-24.135 241	18.84 (0.13)	0.71 (0.18)	0.14 (0.14)			(-62.4±93.8, -1.4±88.0)	0.82	
21	246.723 424	-24.012 333	18.99 (0.09)	0.20 (0.23)	-0.16 (0.12)	17.321 (0.32)	0.54 (0.50)	(95.0±103.5, -35.6±105.9)	0.66	PM
22	246.683 994	-24.138 271	19.62 (0.15)	0.18 (0.27)	-0.35 (0.21)	17.445 (0.30)	1.54 (1.89)	(94.6±153.7, -48.2±123.7)	0.88	PM, multi
22b	246.684 24	-24.137 954	19.46 (0.18)	0.4 (0.23)	-0.13 (0.21)			(101.8±143.9, -36.4±115.1)	0.88	
23	246.830 324	-24.085 192	19.45 (0.14)	0.77 (0.23)	-0.56 (0.20)	15.689 (0.14)	0.84 (0.21)	(-9.2±154.5, 3.6±151.6)	0.68	PM, CH ₄
24	246.664 500	-24.077 206	19.79 (0.18)	1.12 (0.20)	-0.28 (0.23)	15.429 (0.09)	1.04 (0.18)	(-38.8±157.2, 62.6±132.6)	0.82	PM
25	246.663 372	-24.047 895	19.13 (0.11)	-0.23 (0.22)	-0.33 (0.16)	17.159 (0.32)	1.17 (0.85)	(-76.6±129.5, 15.5±116.3)	0.59	PM, CH ₄
26	246.734 655	-24.060 299	19.00 (0.10)	0.30 (0.24)	-0.18 (0.12)	17.116 (0.33)	0.78 (0.50)	(58.2±109.9, 113.0±110.5)	0.82	
27	246.908 266	-24.049 426	19.34 (0.14)	0.97 (0.19)	-0.32 (0.20)	16.005 (0.14)	0.70 (0.19)	(-141.7±179.1, 229.3±196.8)	0.60	CH ₄
28	246.733 341	-24.177 074	19.12 (0.15)	0.62 (0.21)	-0.27 (0.18)	16.576 (0.25)	0.55 (0.33)	(-5.9±128.6, 189.0±134.8)	0.99	CH ₄

Notes. ^athe extinction was obtained from Ridge et al. (2006).

^bPM – proper motion similar with known members within 3 σ .

multi – unresolved objects in the c2d.

CH₄ – potentially strong methane absorption.

H band. We therefore concluded the six rejected candidates should not be T dwarfs.

At the end, with the methane, temperature and brightness criteria discussed above, a total of 28 sources remain as T dwarf candidates in the L 1688 cloud. They are listed in Table 3, giving the coordinates, WIRCam H , $H - K$, and $R_{1.6}$, along with the IRAC/c2d [4.5], [3.6] - [4.5] measurements, and A_{K_s} from the extinction map, followed by the comments in the last column. Unlike young late-M and L dwarfs, no unambiguous T type objects have been identified so far in star-forming regions. Without intrinsic colours of T dwarfs at such young ages, it is difficult to estimate the extinction towards each candidate reliably. We estimated the extinction of each candidate with the extinction map derived by the COMPLETE project (Ridge et al. 2006).

Fig. 7 shows the images of our candidates in H , CH₄ON, IRAC1 and IRAC2. For candidate no. 17, 20, and 22, close companions were found in the WIRCam images but unresolved in the c2d data. Since these companions were as faint as the candidates in WIRCam, we could not attribute the main flux contribution in c2d. None of the three visual companions satisfied our T dwarf selection criteria. The companion 20b was rejected by either T zone, and 17b was not in the temperature T zone. Although 22b was located in both T zones, its $R_{1.6}$ was not reliable given its photometric error. These companions are also listed in Table 3 for future study.

In ρ Oph, one L4 ($K = 15.7$ mag; Alves de Oliveira et al. 2012) and one early-T dwarfs ($K = 17.1$ mag; Marsh et al. 2010a) were reported, suggesting an L/T transition around $K = 17$ mag. Our

candidates are 1.5–2 mag fainter, so with later spectral types. Brown dwarfs have similar radii (Burrows & Liebert 1993). If cloud formation in the atmosphere is not considered, the brightness depends largely on the surface temperature. Scaling with the L4 source with a surface temperature ~ 1650 K (Alves de Oliveira et al. 2012), our T dwarf candidates, if indeed at the distance of ρ Oph, should have surface temperatures ~ 1100 –650 K. Note that even though our candidates have been selected solely with infrared colours, they follow roughly the 1-Myr isochrones of the COND (Baraffe et al. 2003) or of the BT-Settl (Allard, Homeier & Freytag 2012) model, as seen in the CMDs in Fig. 6.

Note that our identification of T dwarfs relies on detection of the methane absorption features, i.e. for methane dwarfs. Because of the time dependence of the properties, e.g. size, temperature, spectral type, and luminosity, of a brown dwarf, the selection criteria based on the field population may not be applicable readily to the young population. Gravity, for example, may play an important role in cloud formation, temperature profile, and CO-CH₄ chemistry in the atmosphere (Marley et al. 2012). Methane absorption in young brown dwarfs with low gravity may appear at cooler temperatures than field T dwarfs do. While this is substantiated by the observations of the exoplanets HR 8799bcd, whose atmospheres are expected to be as cool as field T dwarfs yet show no sign of methane absorption, the planet HR 8799e seems to show methane absorption (Oppenheimer et al. 2013). In addition, two controversial T dwarfs are found, in Orion (Zapatero Osorio et al. 2002, S Ori 70), and in ρ Oph (Marsh et al. 2010a). A confirmed sample of methane sources

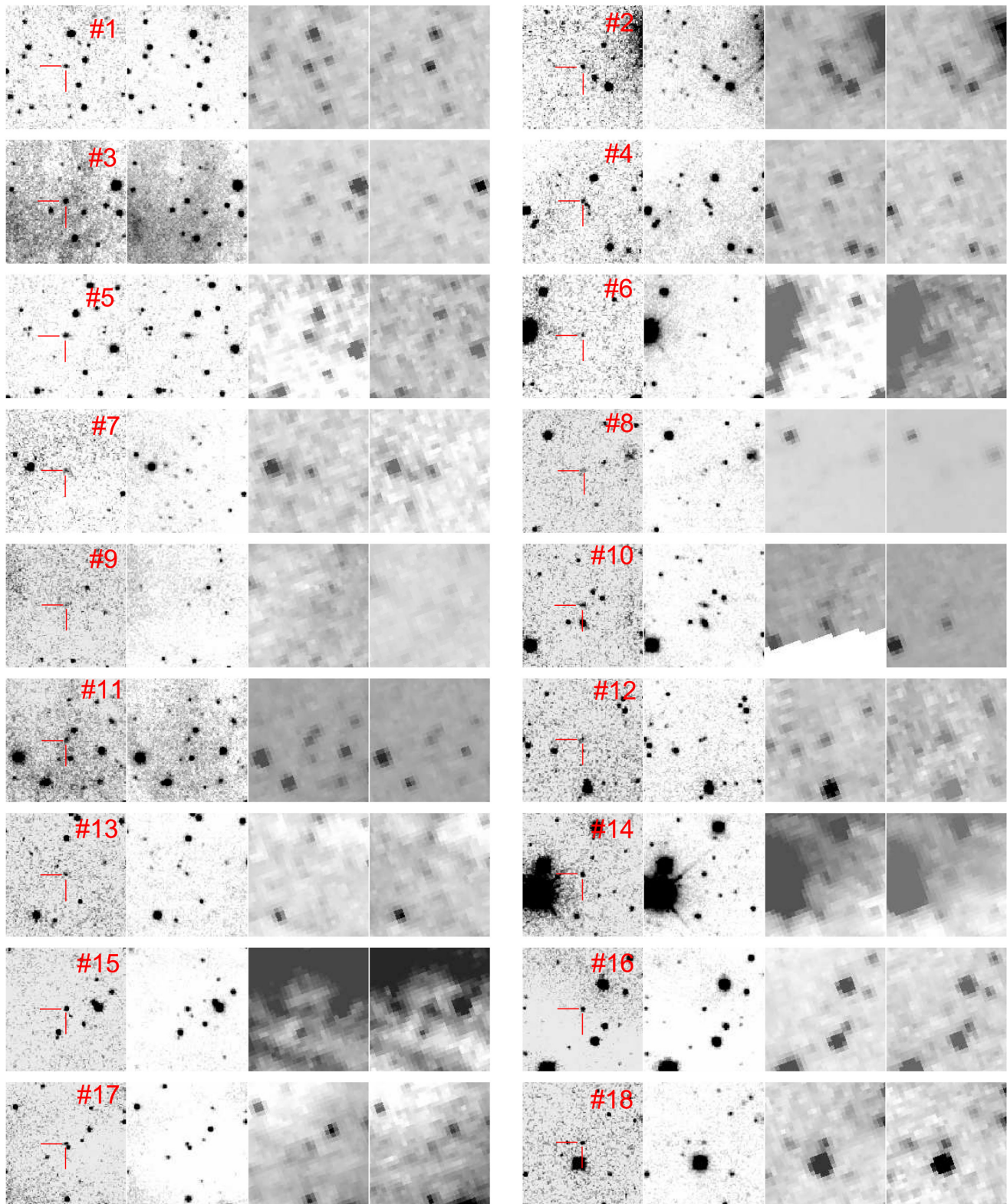


Figure 7. Finding charts of T dwarf candidates. For each candidates, the images of H , CH_4ON , IRAC1, and IRAC2 are shown from left to right, respectively. The size of each image is $16.5 \text{ arcsec} \times 16.5 \text{ arcsec}$. North is up and east is left.

in ρ Oph would thus shed light on the formation and early evolution of the coolest brown dwarfs or even planetary-mass objects.

Kinematics provides possible further constraints of membership. The young stars in the region have an average UCAC2 proper mo-

tion $(\mu_\alpha \cos \delta, \mu_\delta) = (-11.4, -24.5) \text{ mas yr}^{-1}$ (Makarov 2007). We collected the PPMXL proper motions (typical errors 4–10 mas yr^{-1} ; Roeser, Demleitner & Schilbach 2010) of the spectroscopically confirmed young stars in Erickson et al. (2011), and derived

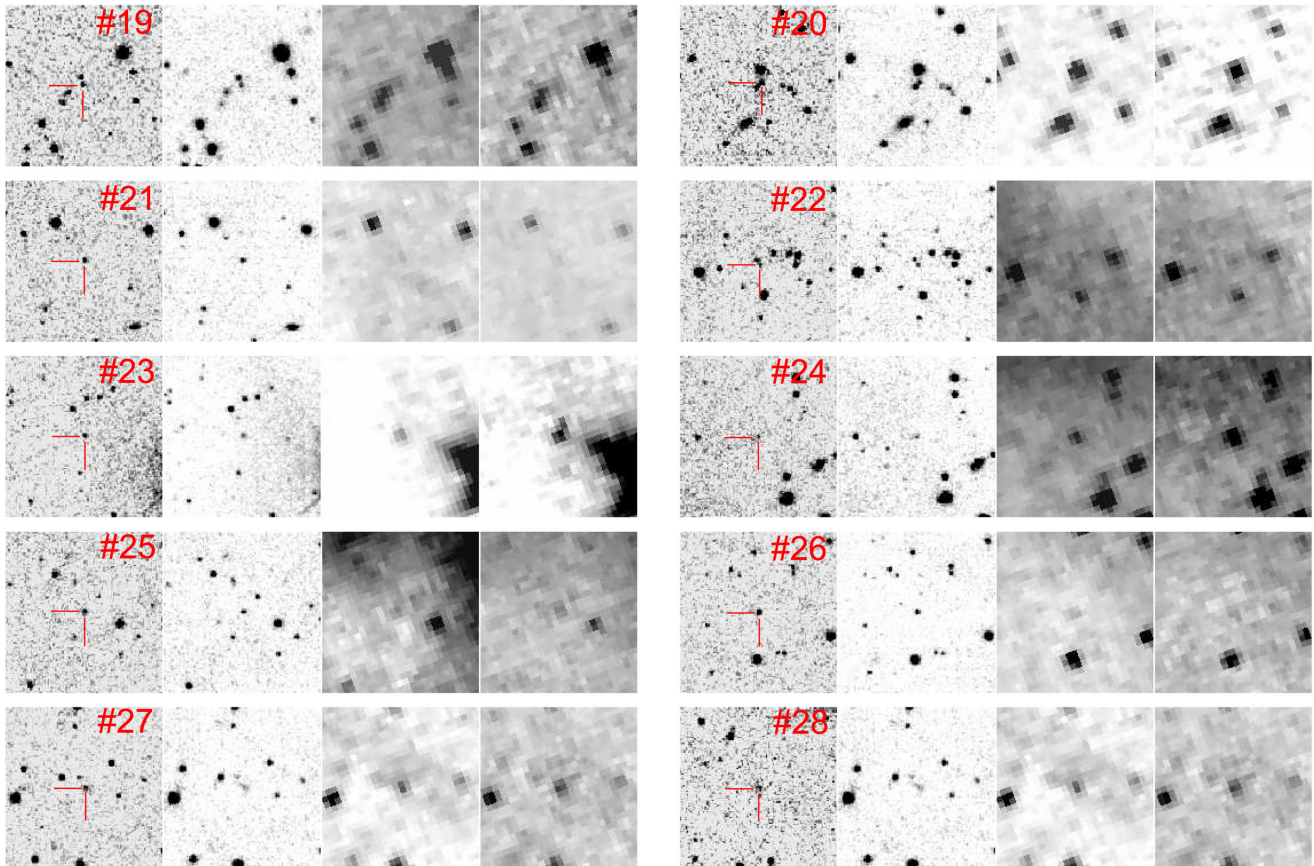


Figure 7 – continued

consistent average values $(\mu_\alpha \cos \delta, \mu_\delta) = (-7.4, -28.4)$ mas yr⁻¹. All these young stars are too bright to measure the positions in our WIRCam images. The proper motions of our WIRCam objects were derived by subtracting the astrometric calibrated positions reported by *daofind* in the *H* band and in the methane images with a 4.3-yr time baseline. The errors of proper motions were derived from the position errors reported by *daofind*. As shown in Fig. 8, while most objects scatter around the origin within 0.1 arcsec in 4.3 yr, the M/L dwarfs display a concentrated distribution, with a slight offset from that of the young stars in the region. In comparison, the T dwarf candidates, being fainter, are more scattered. Even with the large proper motion errors, the 10 candidates in the upper-left corner may not be ρ Oph members.

Fig. 9 shows the spatial distribution of our 28 T dwarf candidates. Because of the high extinction, the T candidates can be found only away from the densest parts of the cloud, outlined by the extinction map based on the 2MASS data (Ridge et al. 2006), but otherwise not randomly distributed as background sources would have been. For example, no candidate is found to the east of the cloud where the extinction is the lowest. We will discuss the contamination issues in the next section.

3.3 Gemini follow-up observations

We have been granted observation time, including spectroscopic and narrow-band imaging, with Gemini North in 2012. Two T dwarf candidates reported by Marsh et al. (2010b) and by Haisch et al. (2010) have been taken their spectra with GNIRS run (see Section 5). Our candidates were observed in narrow-band imaging

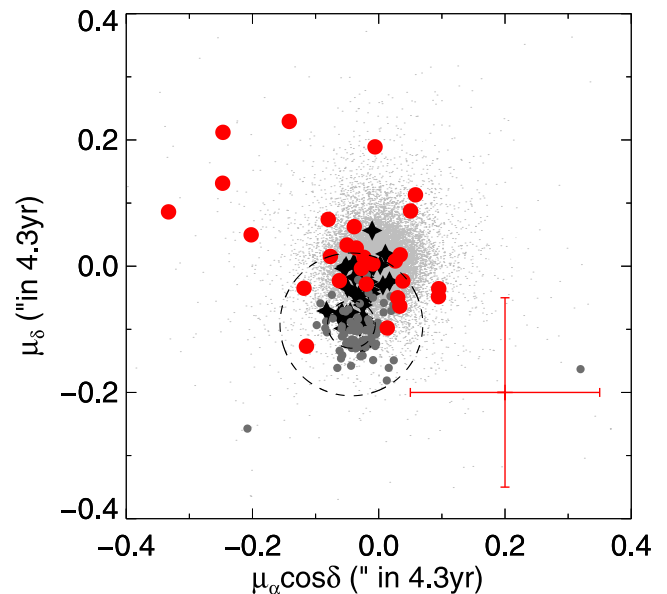


Figure 8. The proper motions of ρ Oph sources (grey dots). Filled asterisks are confirmed late-M and L dwarfs in Geers et al. (2011), Mužić et al. (2012), Alves de Oliveira et al. (2010), and Alves de Oliveira et al. (2012). Dark grey points are confirmed young stars of ρ Oph (Makarov 2007; Erickson et al. 2011). The dashed circles are concentric on the mean proper motion of young stars with 1σ and 3σ radii. T dwarf candidates are marked in red filled circles whose typical proper motion error is represented by the cross.

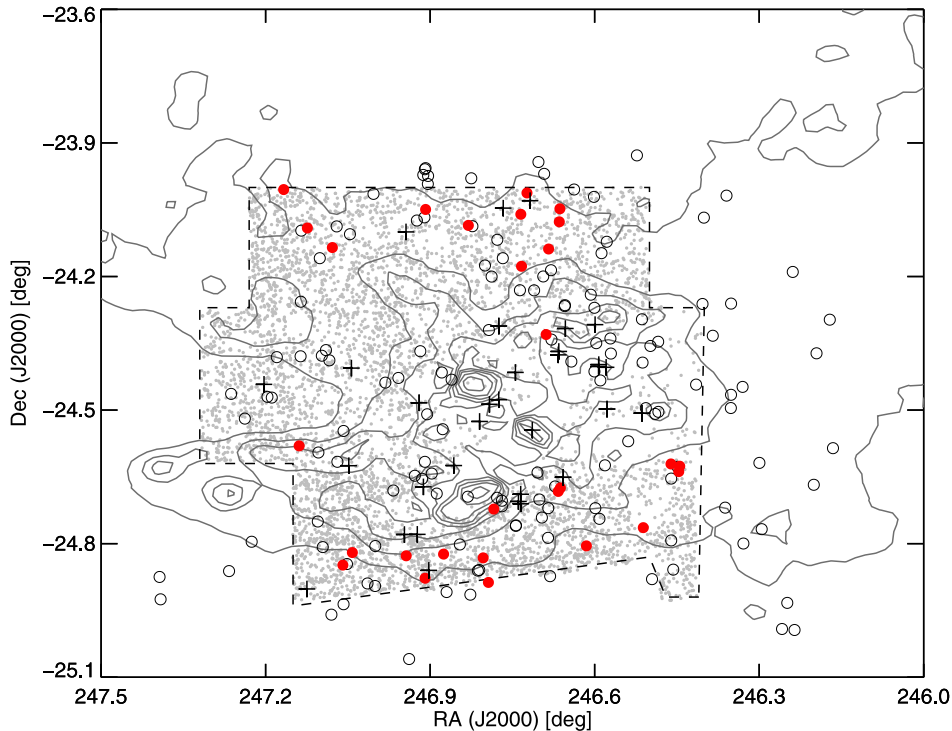


Figure 9. Spatial distribution of our T dwarf candidates (red filled circles), confirmed late-M and L dwarfs (pluses) in Geers et al. (2011), Mužić et al. (2012), Alves de Oliveira et al. (2010), and young stellar members (open circles) listed in Erickson et al. (2011). The grey contours represent the extinction taken from the COMPLETE project (Ridge et al. 2006). The dashed line shows the sky coverage of our observations. Grey dots are objects fainter than 18 mag in the K_s band.

Table 4. Follow-up Gemini observations of T dwarf candidates in ρ Oph.

Object	Instrument	Exposure dither \times exposure \times co-add(s)	Date of observation (UT) (yyyy mm dd)
M10-2776	GNIRS	$8 \times 45 \times 2$	2012 Apr 19
H10-16	GNIRS	$8 \times 90 \times 3$	2012 Apr 23
No. 11	NIRI	Hcon: $7 \times 280 \times 1$, [Fe II]: $7 \times 140 \times 1$, CH ₄ long: $7 \times 50 \times 3$	2012 Jul 23
No. 17	NIRI	Hcon: $13 \times 280 \times 1$, [Fe II]: $13 \times 140 \times 1$, CH ₄ long: $13 \times 80 \times 1$	2012 Aug 10
No. 8	NIRI	Hcon: $20 \times 280 \times 1$, CH ₄ long: $20 \times 80 \times 1$ [Fe II]: $20 \times 140 \times 1$	2012 Aug 13 2012 Aug 26

with the Near InfraRed Imager (NIRI). The follow-up observations, including spectroscopic and narrow-band imaging, are summarized in Table 4. In this subsection, we present the narrow-band imaging results of our T dwarf candidates.

The NIRI is a 1024×1024 InSb array with $0.12 \text{ arcsec pixel}^{-1}$ on the sky at $f/6$, rendering a field of view about $2 \text{ arcmin} \times 2 \text{ arcmin}$. A set of narrow-band filters, Hcon ($1.57 \mu\text{m}$), [Fe II] ($1.64 \mu\text{m}$), and CH₄long ($1.69 \mu\text{m}$), was used for tracing methane absorption in $1.6 \mu\text{m}$, as illustrated in Fig. 1. Raw images were reduced with the GEMINI package under IRAF, and aperture photometry was done with *apphot*. We did not calibrate the instrumental magnitudes of the narrow-band observations to any photometric system. The goal of our narrow-band observations was to check methane absorption. Therefore, we performed a differential photometry rather than absolute photometric calibrations.

Three of our T dwarf candidates (no. 8, 11, and 17) were observed. The candidate no. 8 was selected because it is red and close to a dense region. No. 11 was selected because it is red and is surrounded with nebula. No. 17 was selected because of the agreement with isochrones. No. 8 is not seen in Hcon or [Fe II] but is detected

in CH₄long. The candidate No. 11 is not seen in Hcon, barely visible in [Fe II], and has an extended morphology in CH₄long. Based on available data, the nature of the two candidates are therefore uncertain. The candidate no. 17 was detected in all images, allowing further analysis.

In the field of no. 17, five stars were selected as comparisons. Instrumental magnitudes of [Fe II] and CH₄long were linearly fitted to their Hcon instrumental magnitudes. The differential magnitudes of no. 17 were $\text{Hcon} - [\text{Fe II}] = -0.12 \pm 0.07$ and $\text{Hcon} - \text{CH}_{4\text{long}} = -0.33 \pm 0.06$, consistent with the CFHT result ($R_{1.6} = -0.41 \pm 0.17$) within errors. Fig. 10 shows the NIRI narrow-band images of these three candidates in Hcon, [Fe II], and CH₄long bands.

4 CONTAMINATIONS OF THE SAMPLE

4.1 Galactic contamination

Possible causes of contamination of our candidate sample include stellar variability, photometric errors, and extragalactic sources. As

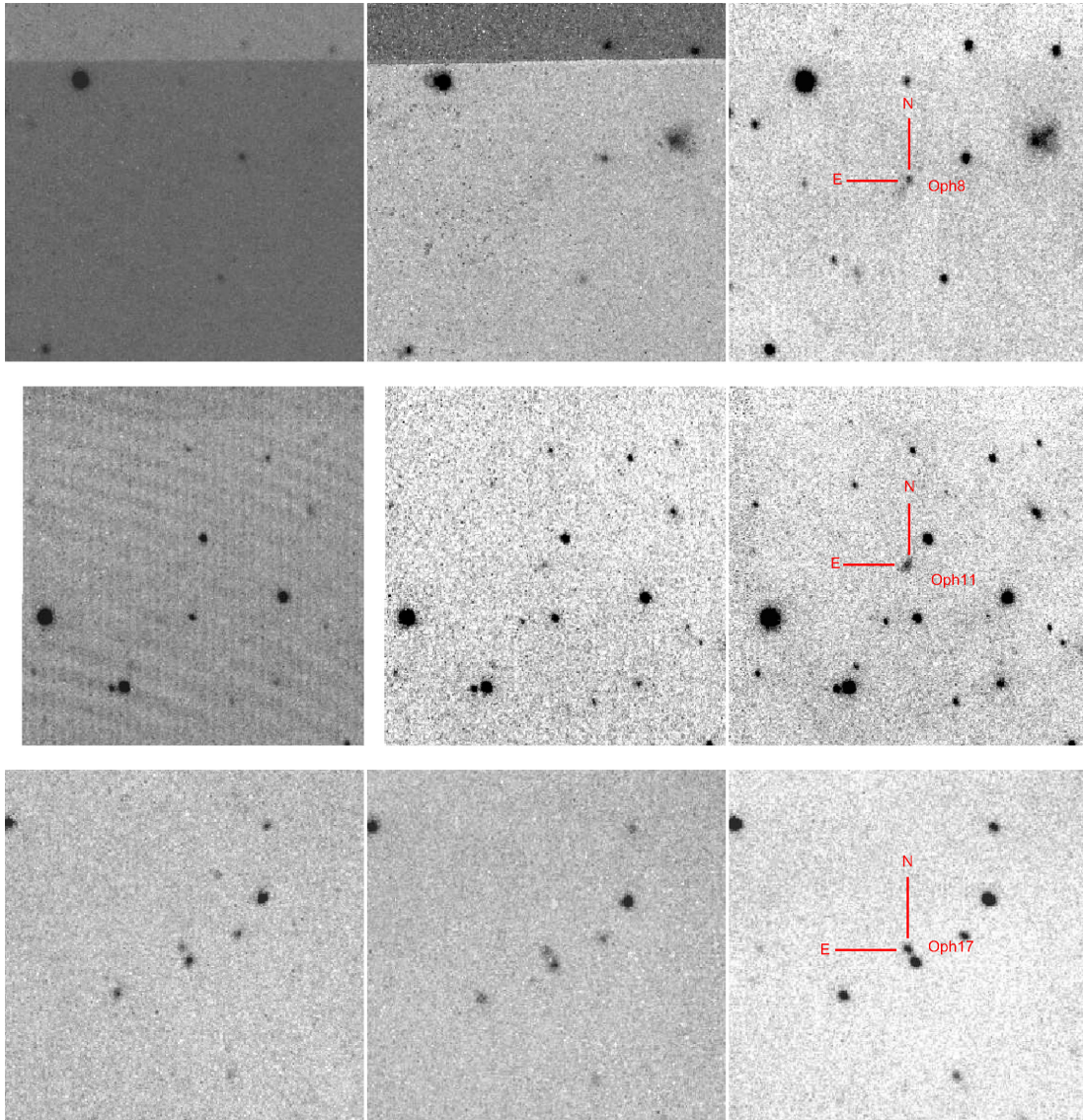


Figure 10. The narrow-band images of T dwarf candidates no. 8 (top), no. 11 (middle), and no. 17 (bottom) in, from left to right, Hcon, [Fe II], and CH₄long. All images are 35 arcsec × 35 arcsec across, with east to the left and north to the top.

a reference field, we chose a 25 arcmin × 25 arcmin low-extinction region (α : 247.738 921 deg, δ : -24.281 188 deg) located about 1 deg from our ρ Oph field, for which *JHK* data are available by WIRCam (images provided by Yan, private communication) and by *UKIDSS*. The field has been also covered by the c2d survey. The WIRCam photometry was derived in a similar way as our own ρ Oph data. In cross-matching of the WIRCam, *UKIDSS* and c2d catalogues, 3014 sources were found with a limiting magnitude ~ 0.5 mag brighter than our ρ Oph sample. The reference field does not have methane observations (no $R_{1.6}$ values), so we used $H_{UKIDSS} - H_{WIRCam}$ to estimate how stellar variability or photometric uncertainties could have led to false positives in the selection by the methane indices.

To estimate the effect of extinction, we distributed the 3014 sources detected in the reference field randomly into our ρ Oph field, using the extinction map of A_K given by COMPLETE (Ridge et al. 2006), and adopting the extinction law (Chapman et al. 2009) at H , 3.6 μ m, and 4.5 μ m. Fig. 11 shows the two-colour and colour-

magnitude diagrams of the reference field. One sees that the reddened field population (in black), which should consist predominantly of Galactic stars, displays a similar distribution as our ρ Oph sample (yellow contours). This verifies that the reference field is a good representation of the field contribution in ρ Oph. There are 114 sources that fall within the methane T zone and 44 sources in the temperature T zone, but none in both; the combination of both methane and temperature/spectral indices effectively windows out interlopers.

Our candidate list may contain foreground T dwarfs or young stars in ρ Oph. Given the T dwarf space density from Reylé et al. (2010) and Kirkpatrick et al. (2012), and multiplying the volume of the cone of 1 deg² out to 130 pc, there may be one foreground T dwarf in our sample. A young star 2MASS 16263682-2419002 is found to have $R_{1.6} = -1.6$ and $[3.6] - [4.5] = 1.16$, indicating strong methane absorptions, and is near the boundary of the temperature T zone. This young star, with an optical spectral type M3.25 (Alves de

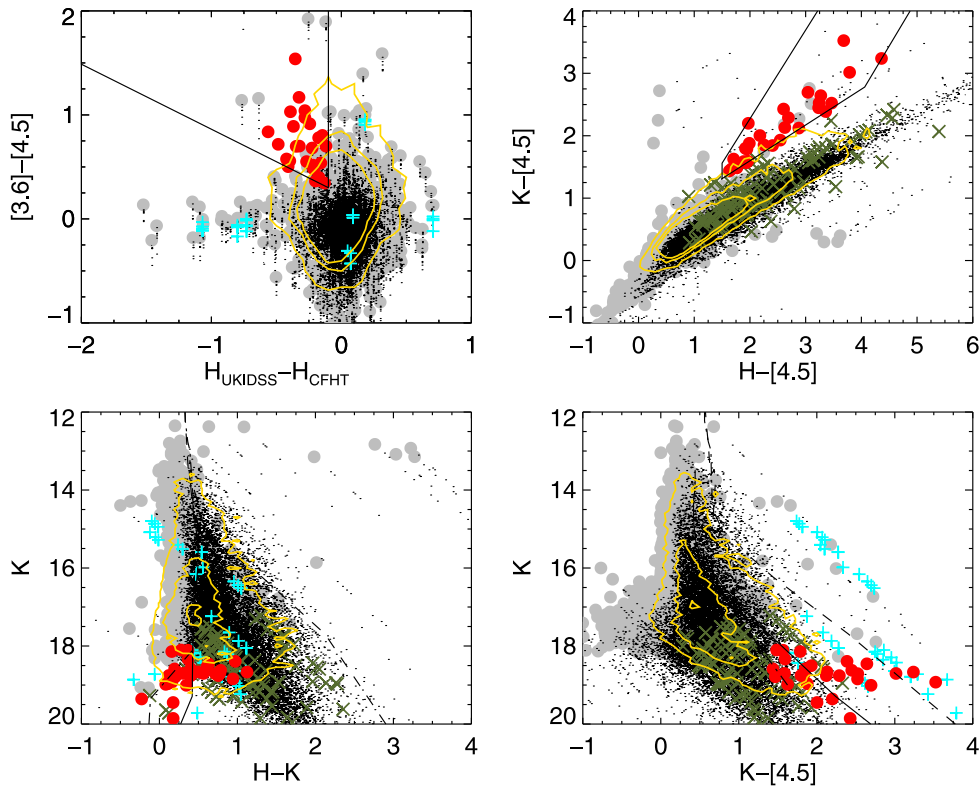


Figure 11. Top: two-colour diagrams and (bottom) CMDs of the reference field. Grey points show the original distribution and black dots are the same stars after applying ρ Oph reddening. Yellow contours represent the distributions of ρ Oph sources. It is seen that the distribution of the reddened background sources is very similar to that in ρ Oph. The cyan pluses are objects (44) located inside the temperature T zone, whereas the green crosses are objects (114) in the methane T zone. Also shown, as in Fig. 6, are our T dwarf candidates (red filled circles) and the 1-Myr isochrones by different models.

Oliveira et al. 2012), has been found to display a large photometric variability ($\Delta K \sim 3.5$ mag) on a time-scale of a year (Alves de Oliveira & Casali 2008). We observed the star with NASA’s 3-m Infrared Telescope Facility (IRTF), on 2011 March 31. Using SpeX (Rayner et al. 2003), a low-resolution (R 120) near-infrared (1–2.5 μm) spectrum was obtained with a 0.5 arcsec width slit in prism mode, under excellent weather condition (seeing ~ 0.35 arcsec). Raw data were processed and calibrated with the *Spextool* pipeline (Cushing, Vacca & Rayner 2004). HD 145127, an A0 star, was used for telluric and flux calibrations with the technique described in Vacca, Cushing & Rayner (2003). The spectrum (see Fig. 12) shows prominent CO lines in the K band, characteristics of low-mass young stellar objects (Greene & Lada 1996). Without the methane absorption, we therefore conclude 2MASS 16263682–2419002 is a low-mass young star, rather than a T dwarf. The false methane detection for this star therefore should be caused by photometric variability. Other kinds of substellar objects, namely late M and L dwarfs, with no methane features, may still be selected if they are photometrically variable.

4.2 Extragalactic contaminations

Extragalactic sources, such as star-forming galaxies, AGNs, or QSOs, share similar positions with T dwarfs in our colour–colour diagrams. Fig. 13 shows our analysis of possible extragalactic contamination. We used the AGNs identified in the GOODS fields by Treister et al. (2006) to estimate the possible number of AGNs detected by *c2d*. There are 316 AGNs in the ~ 0.1 deg² GOODS

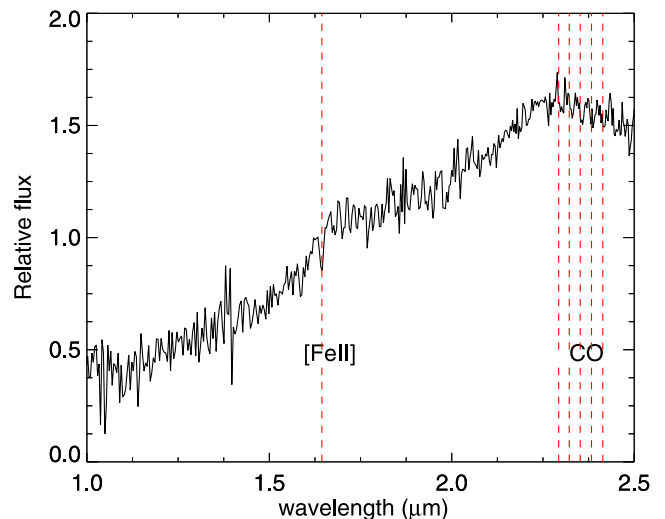


Figure 12. The SpeX near-infrared spectra of 2MASS 16263682–2419002. The CO lines are clearly seen but no methane absorption is found. Therefore, the variability and infrared excess make it behaving like a T dwarf in our selection method. Though this source is excluded by the criterion of MIPS brightness threshold, fainter young objects may still contaminate our sample.

field. We split the extinction map of ρ Oph (Ridge et al. 2006) into 0.1 deg² grids and randomly distribute the AGNs in each grid by 10 000 times. For each realization, an extinction is added to an

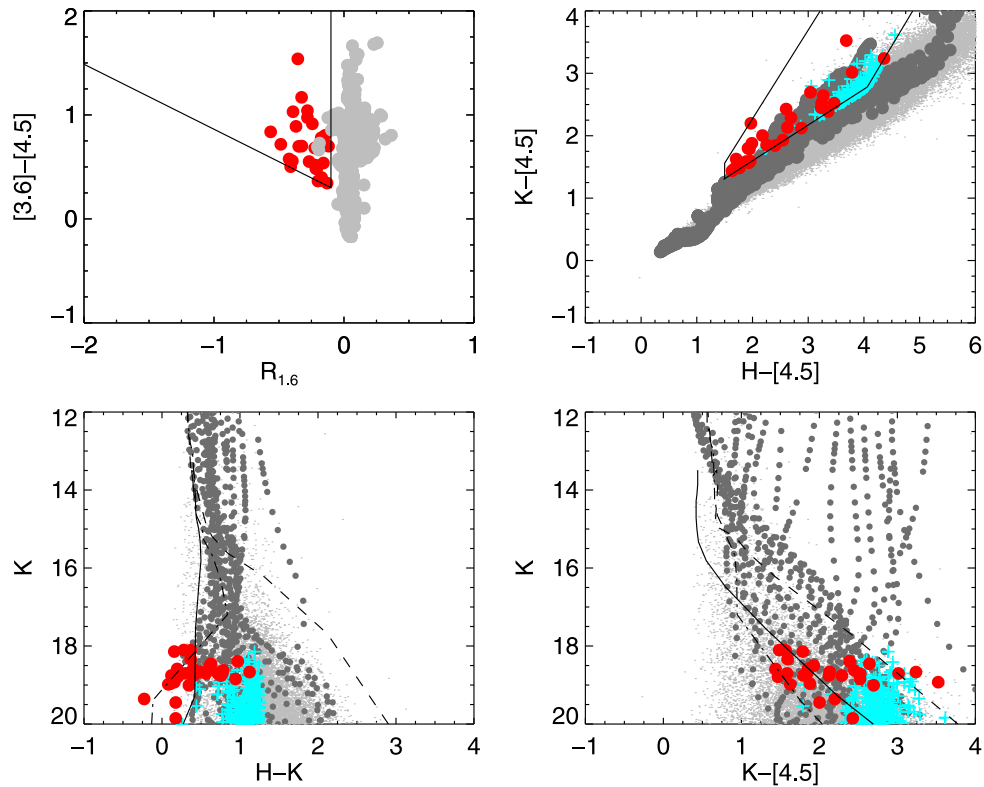


Figure 13. Two-colour diagrams and CMDs of extragalactic sources. In the two-colour diagrams, dark grey dots show the AGN synthetic colours from Polletta et al. (2007) and light grey dots are the SPUDS sources after adding ρ Oph extinction. Plus signs (in cyan) shows the SPUDS sources selected in our analysis without the $R_{1.6}$ criterion. Filled circles (in red) are our T dwarf candidates. The 1-Myr isochrones predicted by different models are symbolized as Fig. 6.

AGN according to its location in the map. Using the faintest T-dwarf candidate ($[4.5] = 17.7$) as the brightness threshold, we found 497 AGNs that would have been detectable by c2d. Assuming a \sqrt{N} statistics, there should be at most 564 AGNs in our field.

To investigate the kinds of AGNs that could pass our selection, we made use of the AGN spectral energy distribution templates by Polletta et al. (2007). Of the 1300 synthesized spectra including 25 kinds of galaxies with redshifts $0 < z < 4$, type-2 QSOs would have been falsely recognized as T dwarf candidates due to the emission lines around $1.5 \mu\text{m}$ at different redshifts. The fraction of such galaxies in ρ Oph is unknown. However, these galaxies would be sufficiently luminous to be detected by MIPS according to the template, so likely not included in our sample.

The Spitzer Public Legacy Survey of the UKIDSS Ultra Deep Survey (SPUDS) observed the UKIDSS Ultra Deep Survey field with *Spitzer* IRAC and MIPS (Dunlop et al. 2007; Kim et al. 2011). Towards high Galactic latitudes, the SPUDS data, dominated by galaxies, provide an alternative estimate of extragalactic contamination in our sample. There are 58 139 sources detected both by UKIDSS and IRAC within the SPUDS field of 0.8 deg^2 , a sky area similar to our ρ Oph field. We added extinction to the SPUDS sample as described before. Without the $R_{1.6}$ measurements for the SPUDS sources, 450 sources (<1 percent) were found within the temperature T zone, and satisfying $[3.6] - [4.5] > 0.3$ with $20 < K < 18$ mag. These sources can potentially contaminate our sample if their $R_{1.6}$ values happen to be less than 0.1 because of photometric uncertainties or variability. Compared to our candidates, these extragalactic sources are redder in $H - K$ (> 0.6) and $K - [4.5]$ (> 2) colours, and do not follow the isochrone. There are 12

candidates in our sample with $H - K < 0.6$ and $K - [4.5] < 2$, i.e. clearly distinguishable from extragalactic sources.

To summarize, most background stars could be ruled out by the temperature/spectral type criterion, i.e. in the $H - [4.5]$ versus $K - [4.5]$ diagram. There is a chance of one field T dwarf in the sightline to ρ Oph. As shown in Fig. 13, while 16 candidates shared similar colours ($H - K > 0.6$ or $K - [4.5] > 2$) with galaxies, the rest 12 candidates have distinctly different colours. We therefore conclude that extragalactic sources should contribute to roughly half of false detections. This leaves still a sizeable fraction of valid candidates in our sample.

5 COMPARISON WITH PREVIOUS STUDIES

Alves de Oliveira et al. (2010) selected substellar candidates using *JHK* colours and the 1-Myr isochrone predicted by the DUSTY model (Chabrier & Baraffe 2000). Among their 110 candidates, 32 have been confirmed late-M to L 4 dwarfs in their follow-up spectroscopic observations (Alves de Oliveira et al. 2010, 2012). The L 4 dwarf is particularly relevant because it anchors the upper limit in brightness; any T dwarf in ρ Oph should be fainter ($K > 16$ mag). Geers et al. (2011) identified two samples of low-mass candidates in ρ Oph, one with colours redder than the 1-Myr COND isochrone in the *i* versus *i* - *J* CMD, and the other with $J - K > 1.5$ mag and with infrared excess in the c2d data. In their follow-up spectroscopic observations of more than one hundred candidates, most turned out to be background stars and 23 were spectroscopically confirmed low-mass stars or brown dwarfs (Geers et al. 2011; Mužić et al.

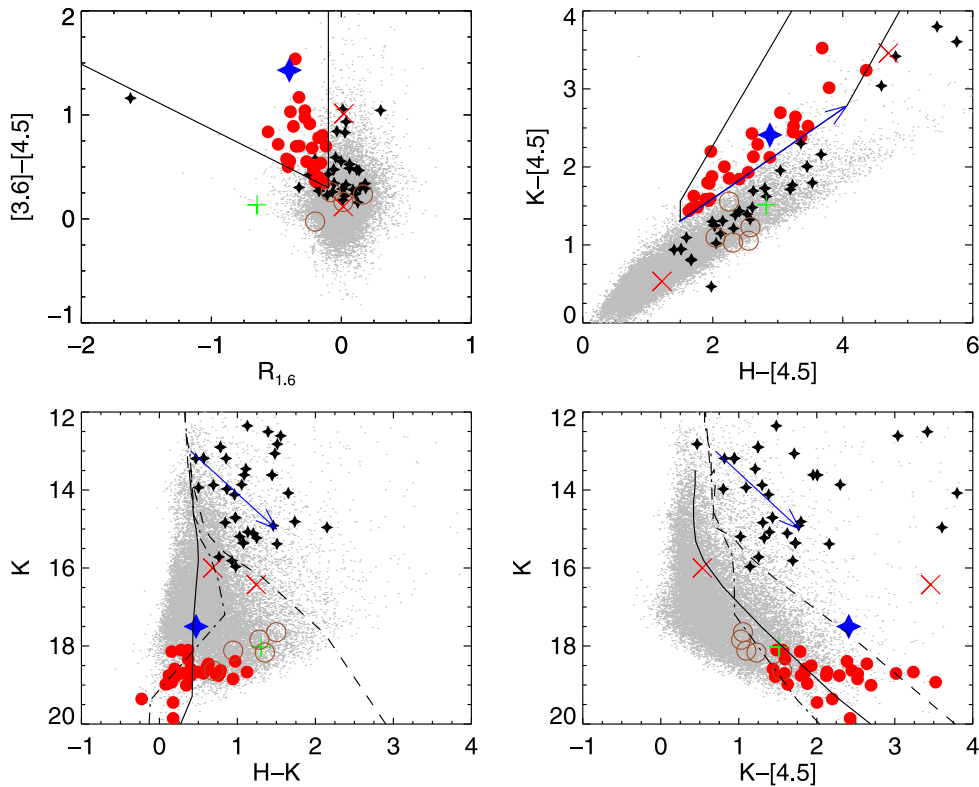


Figure 14. Published low-temperature candidates in our two-colour and colour–magnitude diagrams. Red crosses: Barsony et al. (2012). Green pluses: Marsh et al. (2010b). Brown circles: Haisch et al. (2010). Our candidates are shown in red filled circles. Also shown are the confirmed late-M and L dwarfs in ρ Oph (in black asterisks), the T dwarf S Ori 70 (Zapatero Osorio et al. 2002, in blue asterisk) in σ Orion, scaled to the distance of ρ Oph. The 1-Myr isochrones predicted by different models and the reddening vector are the same as Fig. 6. Grey dots are all objects in our catalogue.

2012). In total, there are 49 confirmed low-mass stars or brown dwarfs in the region.

Except bright stars or stars out of our field, all the confirmed low-mass stars or brown dwarfs (32) are in our WIRCam plus c2d merged catalogue. All these confirmed objects were found to be variable either by Alves de Oliveira & Casali (2008) or by the photometric measurements we collected in the literature. In addition, 13 confirmed objects have proper motions consistent (within 1σ) with those of the young stars (Makarov 2007; Erickson et al. 2011). Fig. 14 shows how these confirmed M/L objects behave in our diagnosis diagrams. Those that happen to be located in the methane T zone would have been excluded from the temperature T zone because of their high temperatures. The M/L objects are on or redder than the DUSTY isochrone, while our T candidates are bluer and fainter. Our sample, selected by brightness and colours without a priori constraints with any atmospheric model, are found clustered around the 1-Myr COND isochrone, reassuring of the T dwarf nature. This explains why our sample and that of Alves de Oliveira et al. (2010) are exclusive of each other.

Marsh et al. (2010b) and Barsony et al. (2012) selected candidates of low-mass stars and brown dwarfs by fitting photometric data (J , H , K , $[3.6]$, and $[4.5]$) to atmospheric models. The surface temperatures of their candidates are mostly higher than 1500 K. Those cooler than 1500 K, i.e. T dwarf candidates, will be discussed in the next section. Fig. 15 shows our H and K magnitudes to be consistent with those by Alves de Oliveira et al. (2010), and by Marsh et al. (2010b). The K -band measurements by Barsony et al. (2012), however, are systematically brighter for candidates

fainter than ~ 17 mag. The reason for this discrepancy is unknown. With an over estimated K -band brightness, these sources would have been classified as brown dwarf candidates. Using our photometry, however, these candidates should be background stars.

Among the brown dwarf candidates listed by Marsh et al. (2010b), those with $K \gtrsim 16$ mag and with surface temperatures cooler than 1500 K are relevant to our T dwarf work. There are eight such sources, five of which are detected by c2d, including the early T dwarf (their star no. 4450) which has $[3.6] - [4.5] > 0.3$, indeed suggestive of methane absorption, but it is too faint in our WIRCam images. Two sources are listed in our merged catalogue: no. 2776 (M10-2776) and no. 5820 (M10-5820), both having $R_{1.6} < -0.1$. M10-5820 has $[3.6] - [4.5] < 0.3$ and is not in our temperature T zone. M10-2776, while being in both T zones, is detected by MIPS. They both therefore are not included in our candidate list.

Using the same brightness ($K \gtrsim 16$ mag) and temperature ($\lesssim 1500$ K) conditions, we should have found seven T dwarf candidates in the list of Barsony et al. (2012). Fig. 16 shows the finding charts. None of these are in the methane T zone. Our photometry of no. 877 (B12-877) ($H \sim 16.68$ mag, $K \sim 16.00$ mag) is some 1 mag brighter than reported by Barsony et al. (2012). According to its position in the CMDs, B12-877 is likely a background source. No. 272 (B12-272) shows $[3.6] - [4.5] = 1.01$, but its $[4.5]$ ($=12.97$ mag) is too bright to be a T dwarf. However, in the CMDs, B12-272 is close to the DUSTY 1-Myr isochrone, so we cannot rule out its being an L or early T dwarf. No. 181 (B12-181) is excluded from our data because it is not listed in c2d. B12-430 has no counterpart within 2 arcsec radius of any source in our merged catalogue. No. 886

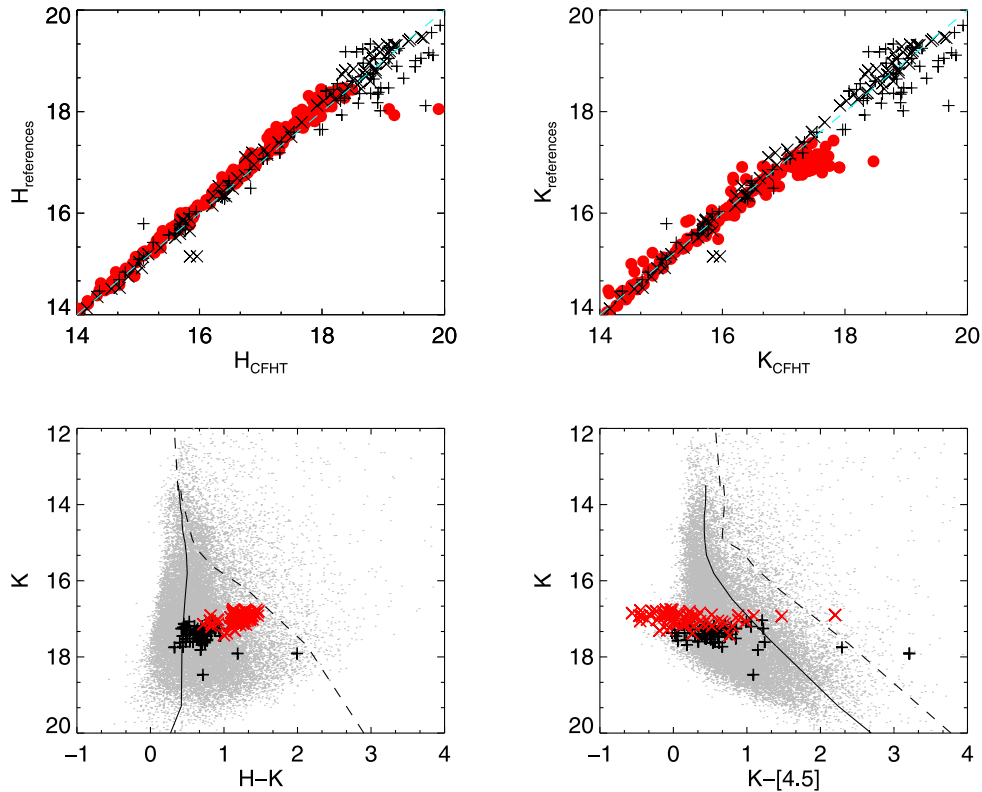


Figure 15. Top: the photometric measurements of brown dwarf candidates in H (left) and K (right) band. Our measurements by CFHT are on the x -axis, and magnitudes from different authors are on the y -axis in pluses (Alves de Oliveira et al. 2010), crosses (Marsh et al. 2010b), and filled circles (Barsony et al. 2012). Note the discrepancy between our measurements and the measurements from Barsony et al. (2012) beyond $K > 17$. Bottom: the CMDs of faint ($K > 17$) candidates in Barsony et al. (2012). Pluses represent our measurements and crosses are from Barsony et al. (2012). The 1-Myr isochrones of COND and DUSTY models are shown in solid and dashed lines, respectively.

(B12-886) is close to 2MASS 16281471–2428325 and has neither WIRCam nor c2d counterpart. For B12-425 and B12-572, each has two faint counterparts with a neighbouring bright star. There could be confusion between the c2d and NIR sources.

With methane on–off imaging, Haisch et al. (2010) selected 22 T dwarf candidates showing possible methane absorption at 1.6 μm . We found seven counterparts in our merged catalogue within 2 arcsec radius, but none are in both T zones. Their colours suggest background stars or extragalactic sources. In Table 5, we list the T dwarf candidates identified in previous studies (Haisch et al. 2010; Marsh et al. 2010b; Barsony et al. 2012) and detected in our WIRCam images or in c2d catalogue. The first two columns are the coordinates of the sources, followed by the H and K magnitudes reported by the respective group. Our WIRCam measurements are in parentheses. The next three columns give the $R_{1.6}$, [4.5], and [3.6] – [4.5] data. The last column is the identification of the source, e.g. M10-2776 means star number 2776 in the compilation of Marsh et al. (2010b).

5.1 Gemini spectroscopic observations on H10-16 and M10-2776

Low-resolution ($R \sim 540$) spectra of the two T dwarf candidates, M10-2776 and H10-16, were obtained, using the 32 l/mm grating SXD prisms and 1 arcsec wide slit with GNIRS. The cross-dispersed spectra of order 3 (1.9–2.5 μm) and of order 4 (1.4–1.8 μm) were used to detect possible methane or water absorptions.

The source H10-16 shows possible 1.6- μm methane absorption in both methane on/off imaging surveys, 3.3- μm methane absorption in the [3.6] – [4.5] colour from the c2d catalogue, and is located near the 1-Myr BT-Settl isochrone in the $K - [4.5]$ versus K CMD. However, it is excluded as a T dwarf candidate by the temperature criterion. The GNIRS spectrum of H10-16 shows a flat continuum with no methane or water feature (see Fig. 17), therefore should not be a T dwarf.

Another source M10-2776 also shows possible 1.6- and 3.3- μm methane absorptions but is excluded as a T dwarf because of its MIPS detection. The infrared spectrum for M10-2776 (Fig. 17) exhibits a flat continuum with some emission lines, but without methane or water absorptions. Assuming the strongest emission line is $H\alpha$, the spectrum of M10-2776 matches with the QSO spectral energy distribution templates (Polletta et al. 2007), containing emission of $H\alpha$, $H\beta$, and [O III] at $z \sim 2.15$. This demonstrates the usefulness of the MIPS criterion to remove extragalactic sources in our selection.

In addition to M10-4450 (Marsh et al. 2010a), the other young T dwarf claimed by Zapatero Osorio et al. (2002) was S Ori 70 in σ Ori. The status of S Ori 70 as a young, low-gravity T dwarf was questioned by Burgasser et al. (2004), but was substantiated by the new photometric data (Zapatero Osorio et al. 2008). A possible disc was suggested by the redder *Spitzer*/IRAC colours than field T dwarfs (Scholz & Jayawardhana 2008). The proper motion of S Ori 70 is inconsistent with known members of σ Ori (Peña Ramírez et al. 2011). Though the nature of S Ori 70 is

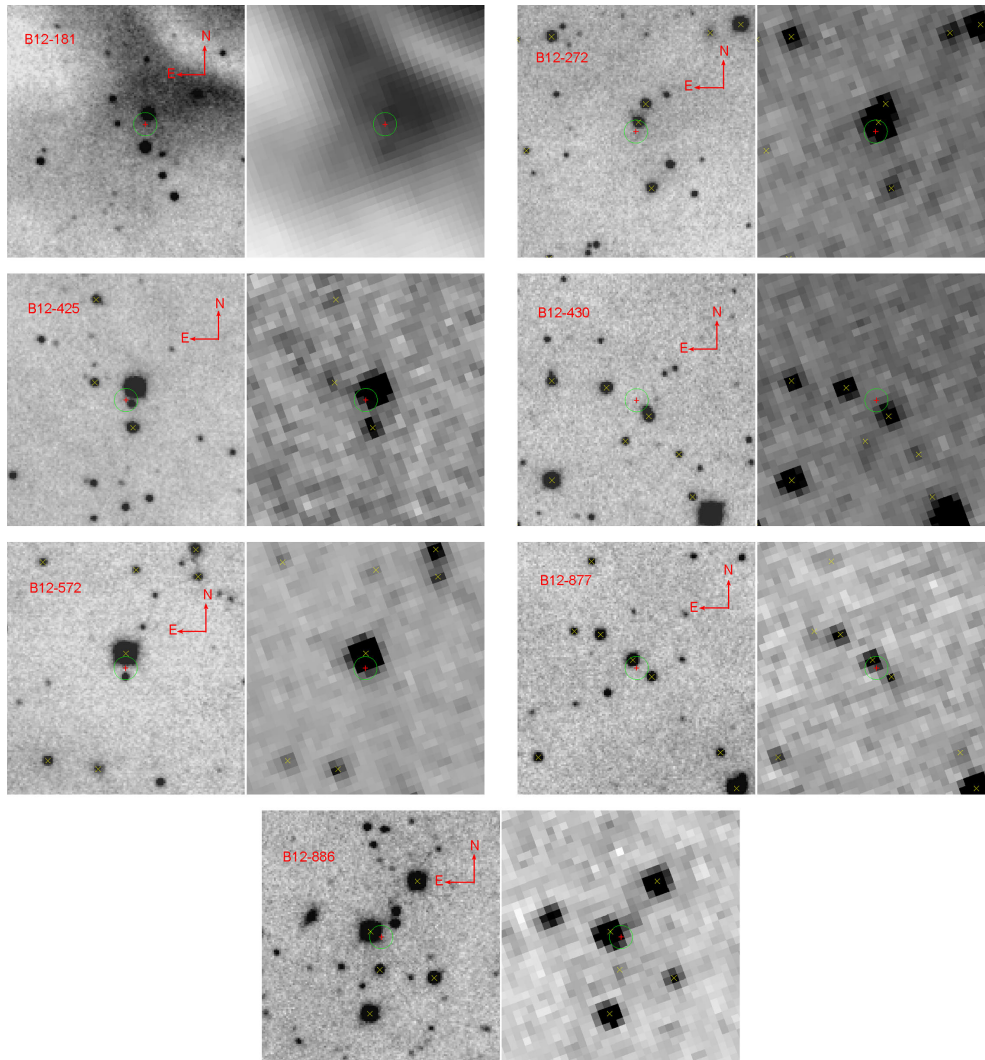


Figure 16. Finding charts of low-temperature candidates in Barsony et al. (2012). For each target, the WIRCcam CH₄ON image is shown on the left and IRAC [4.5] image on the right. The position of each target reported in Barsony et al. (2012) is represented by a red plus, surrounding by a 2 arcsec radius circle. Yellow crosses are sources detected in our merged catalogue. All images are in 41 arcsec \times 43 arcsec.

controversial, it is the only T dwarf close to a star-forming region with multiband photometry of *JHK*, methane on/off, and IRAC data. As seen in Fig. 14, S Ori 70 is located in both T zones. Our method would have identified S Ori 70 as a T dwarf, if it were in ρ Oph.

6 CONCLUSIONS

We have established a set of photometric criteria to find T dwarfs based on the characteristic methane absorptions, cool temperatures, and infrared brightness. With a sample of 28 known L and T dwarfs, the methane on–off imaging is found to be effective in diagnosis of the 1.6- μ m methane absorption beyond T3/T4. Additionally, the *Spitzer*/IRAC [3.6]–[4.5] colour is used for another methane feature near 3.3 μ m. A combination of the two methane indices makes secured identification of the methane feature and against stellar variability or photometric uncertainty. For spectral type and temperature selection, $H - [4.5]$ and $K - [4.5]$ colours are utilized. While young stars, because of their variability, may contaminate the methane selection, they will be excluded by the temperature and brightness criteria. Extragalactic sources comprise the most con-

tributors of contaminations, particularly towards faint magnitudes, though some can be rejected by their mid-infrared MIPS brightness. In the ρ Oph star-forming region, a total of 28 T dwarf candidates are identified, of which about half of which may be confused by QSO/AGN sources. Without a priori selection by any atmospheric models, our candidates are mostly distributed around the 1-Myr COND or BT-Settl isochrones in the CMD. After excluding outliers, about half of our candidates may share the same proper motions with known young stars in the region. The spacial distribution of our candidates are collocated with known young stars. Our selection criteria are the most stringent and conservative in comparison to those in the literature for T dwarfs. Spectroscopic confirmation of even a few of our candidates would enlarge the known sample of young T dwarfs.

ACKNOWLEDGEMENTS

We thank Dr Wei-Hao Wang for the support on the SIMPLE pipeline and Dr Niall Deacon for the help on IRTF observations. The work at NCU is financially supported in part by the grant NSC102-2119-M-008-001. This research has benefited from the M, L, T, and Y dwarf

Table 5. T-like dwarf candidates in selected literature.

RA (deg)	Dec (deg)	<i>H</i> (mag)	<i>K</i> (mag)	<i>R</i> _{1.6} /CH ₄ (s-l) ^a (mag)	[4.5] (mag)	[3.6]–[4.5] (mag)	References ^b
246.857 08	−24.931 472	17.98 ± 0.04 (17.91)	17.16 ± 0.04(17.17)	(−0.22 ± 0.06)	15.08 ± 0.05	–	M10-2776
246.855 63	−24.427 083	18.34 ± 0.05	17.71 ± 0.06	–	15.85 ± 0.10	0.13 ± 0.16	M10-4450
246.833 54	−24.440 528	18.75 ± 0.07	18.04 ± 0.08	–	15.37 ± 0.09	1.30 ± 0.17	M10-5071
246.799 96	−24.446 361	18.66 ± 0.07(19.33 ± 0.20)	17.93 ± 0.07(18.03 ± 0.12)	(−0.65 ± 0.23)	16.61 ± 0.12	0.14 ± 0.18	M10-5820
246.801 50	−24.408 222	19.42 ± 0.13	–	–	16.49 ± 0.15	0.33 ± 0.24	M10-6480
246.544 42	−24.587 861	17.49 ± 0.05(17.23 ± 0.04)	16.46 ± 0.06(16.32 ± 0.03)	(0.10 ± 0.06)	–	–	B12-181
246.647 13	−24.711 361	17.72 ± 0.06(17.67 ± 0.05)	16.28 ± 0.05(16.43 ± 0.07)	(0.02 ± 0.07)	12.97 ± 0.05	1.01 ± 0.08	B12-272
246.805 83	−24.284 306	18.43 ± 0.08(18.38 ± 0.09)	16.99 ± 0.07(17.54 ± 0.07)	(0.03 ± 0.10)	13.33 ± 0.07	−0.03 ± 0.14	B12-425
246.812 42	−24.247 194	17.24 ± 0.05	16.49 ± 0.06	–	15.37 ± 0.11	−0.01 ± 0.16	B12-430
246.967 50	−24.385 972	18.35 ± 0.08(18.28 ± 0.07)	17.07 ± 0.08(17.60 ± 0.05)	(−0.01 ± 0.08)	12.70 ± 0.05	0.08 ± 0.07	B12-572
247.059 46	−24.375 500	17.83 ± 0.06(16.68 ± 0.03)	17.14 ± 0.08(16.00 ± 0.02)	(0.02 ± 0.05)	15.47 ± 0.09	0.12 ± 0.12	B12-877
247.060 75	−24.475 917	17.98 ± 0.06	16.93 ± 0.07	–	13.73 ± 0.06	0.05 ± 0.08	B12-886
246.456 17	−24.333 914	18.58(18.99 ± 0.09)	17.72(18.32 ± 0.11)	−0.23(0.13 ± 0.11)	–	–	H10-1
246.481 50	−24.413 181	19.43(20.31 ± 0.31)	18.15(18.79 ± 0.19)	−0.49(0.27 ± 0.32)	–	–	H10-2
246.483 46	−24.566 928	18.41(18.85 ± 0.08)	17.14(18.24 ± 0.09)	−0.35(0.09 ± 0.11)	–	–	H10-4
246.497 37	−24.271 189	18.87(19.52 ± 0.13)	17.66(18.17 ± 0.19)	−0.27(0.17 ± 0.16)	16.94 ± 0.31	0.23 ± 0.42	H10-5
246.563 50	−24.577 281	18.84(19.12 ± 0.18)	17.64(18.14 ± 0.08)	−0.21(0.00 ± 0.20)	–	–	H10-6
246.611 50	−24.658 258	18.75(19.07 ± 0.10)	17.42(18.42 ± 0.08)	−0.24(0.14 ± 0.14)	–	–	H10-7
246.800 46	−24.286 958	19.15(18.92 ± 0.10)	17.88(18.56 ± 0.09)	−0.46(−0.23 ± 0.11)	–	–	H10-9
246.819 25	−24.376 008	19.37	17.75	−0.26	16.73 ± 0.26	−0.06 ± 0.30	H10-10
246.835 04	−24.320 719	18.80(19.30 ± 0.12)	17.35(17.50 ± 0.07)	−0.76(−0.15 ± 0.15)	16.39 ± 0.19	0.11 ± 0.22	H10-11
246.853 37	−24.642 717	19.17(19.99 ± 0.25)	17.40(17.98 ± 0.09)	−0.56(0.19 ± 0.27)	15.74 ± 0.12	0.34 ± 0.16	H10-12
246.875 75	−24.656 850	18.94(19.30 ± 0.15)	17.17(18.33 ± 0.05)	−0.67(0.02 ± 0.19)	–	–	H10-13
246.888 54	−24.317 683	19.15(19.12 ± 0.11)	17.43(17.84 ± 0.08)	−0.65(−0.20 ± 0.13)	16.81 ± 0.19	−0.03 ± 0.24	H10-14
246.890 46	−24.325 119	18.79(19.14 ± 0.09)	17.40(17.65 ± 0.05)	−0.27(0.01 ± 0.11)	16.59 ± 0.23	0.16 ± 0.26	H10-15
246.899 25	−24.353 631	19.09(19.33 ± 0.11)	18.23(18.63 ± 0.14)	−0.51(−0.18 ± 0.14)	17.08 ± 0.28	–	H10-16
246.923 96	−24.268 025	18.70(19.14 ± 0.09)	17.64(18.02 ± 0.07)	−0.27(0.05 ± 0.12)	–	–	H10-18
246.934 46	−24.350 356	18.84(19.07 ± 0.09)	17.62(18.12 ± 0.07)	−0.24(−0.08 ± 0.12)	17.02 ± 0.24	0.26 ± 0.28	H10-19
247.045 04	−24.484 633	18.84	17.98	−0.41	17.54 ± 0.49	0.22 ± 0.59	H10-20

Notes. ^aThe *R*_{1.6} values are derived by *H* − CH₄ON and CH₄(s-l) values (Haisch et al. 2010) are derived by CH₄s − CH₄l.

^bM10: Marsh et al. (2010b) B12: Barsony et al. (2012), H10: Haisch et al. (2010).

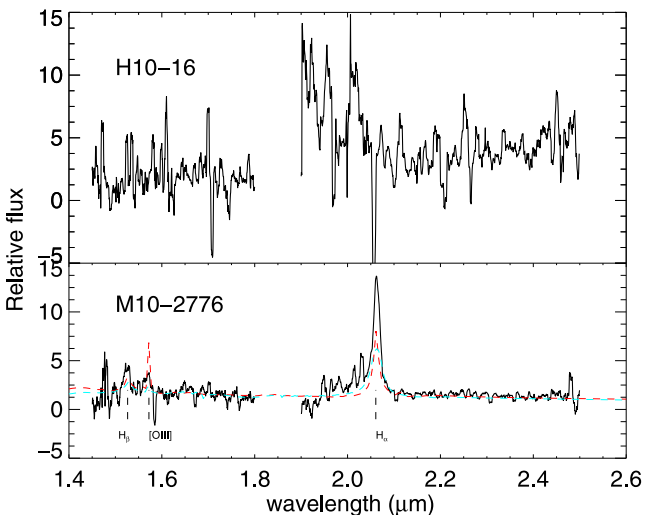


Figure 17. *H* and *K* band spectrum of H10-16 (top) and M10-2776 (bottom). Also shown in curved dashed lines are QSO templates with a redshift *z* ∼ 2.15. The emission lines of H α , H β , and [O III] are indicated with vertical dashed lines.

compendium housed at DwarfArchives.org. This research has benefited from the SpeX Prism Spectral Libraries, maintained by Adam Burgasser at <http://pono.ucsd.edu/~adam/browndwarfs/spexprism>. Based on observations obtained with WIRCam, a joint project of

CFHT, Taiwan, Korea, Canada, France, at the CFHT which is operated by the National Research Council (NRC) of Canada, the Institut National des Sciences de l’Univers of the Centre National de la Recherche Scientifique of France, and the University of Hawaii.

REFERENCES

- Allard F., Homeier D., Freytag B., 2012, *Phil. Trans. R. Soc. A*, 370, 2765
 Alves de Oliveira C., Casali M., 2008, *A&A*, 485, 155
 Alves de Oliveira C., Moraux E., Bouvier J., Bouy H., Marmo C., Albert L., 2010, *A&A*, 515, A75
 Alves de Oliveira C., Moraux E., Bouvier J., Bouy H., 2012, *A&A*, 539, A151
 Baraffe I., Chabrier G., Allard F., Hauschildt P. H., 2002, *A&A*, 382, 563
 Baraffe I., Chabrier G., Barman T. S., Allard F., Hauschildt P. H., 2003, *A&A*, 402, 701
 Barsony M., Haisch K. E., Marsh K. A., McCarthy C., 2012, *ApJ*, 751, 22
 Basri G., 2000, *ARA&A*, 38, 485
 Béjar V. J. S., Zapatero Osorio M. R., Rebolo R., Caballero J. A., Barrado D., Martín E. L., Mundt R., Bailer-Jones C. A. L., 2011, *ApJ*, 743, 64
 Bertin E., Mellier Y., Radovich M., Missonnier G., Didelon P., Morin B., 2002, in Bohlender D. A., Durand D., Handley T. H., eds, *ASP Conf. Ser. Vol. 281, Astronomical Data Analysis Software and Systems XI*. Astron. Soc. Pac., San Francisco, p. 228
 Burgasser A. J., Kirkpatrick J. D., McGovern M. R., McLean I. S., Prato L., Reid I. N., 2004, *ApJ*, 604, 827
 Burgess A. S. M., Moraux E., Bouvier J., Marmo C., Albert L., Bouy H., 2009, *A&A*, 508, 823

- Burrows A., Liebert J., 1993, *Rev. Mod. Phys.*, 65, 301
- Burrows A., Hubbard W. B., Lunine J. I., Liebert J., 2001, *Rev. Mod. Phys.*, 73, 719
- Chabrier G., Baraffe I., 2000, *ARA&A*, 38, 337
- Chapman N. L., Mundy L. G., Lai S. P., Evans N. J., II, 2009, *ApJ*, 690, 496
- Comerón F., Spezzi L., López Martí B., 2009, *A&A*, 500, 1045
- Cushing M. C., Vacca W. D., Rayner J. T., 2004, *PASP*, 116, 362
- Ducati J. R., Bevilacqua C. M., Rembold S. B., Ribeiro D., 2001, *ApJ*, 558, 309
- Dunlop J. et al., 2007, *Spitzer Proposal*, 40021
- Erickson K. L., Wilking B. A., Meyer M. R., Robinson J. G., Stephenson L. N., 2011, *AJ*, 142, 140
- Evans N. J. et al., 2007, *Final Delivery of Data from the c2d Legacy Project: IRAC and MIPS. SSC, Pasadena*
- Geers V., Scholz A., Jayawardhana R., Lee E., Lafrenière D., Tamura M., 2011, *ApJ*, 726, 23
- Greene T. P., Lada C. J., 1996, *AJ*, 112, 2184
- Haisch K. E., Jr, Barsony M., Tinney C., 2010, *ApJ*, 719, L90
- Hayashi C., Nakano T., 1963, *Prog. Theor. Phys.*, 30, 460
- Kim M., Dunlop J. S., Lonsdale C. J., Farrah D., Lacy M., Sun M., SpUDS Team 2011, *BAAS*, 43, 335.51
- Kirkpatrick J. D., 2005, *ARA&A*, 43, 195
- Kirkpatrick J. D. et al., 2011, *ApJS*, 197, 19
- Kirkpatrick J. D. et al., 2012, *ApJ*, 753, 156
- Kumar S. S., 1963, *ApJ*, 137, 1121
- Leggett S. K. et al., 2010, *ApJ*, 710, 1627
- Lodieu N., Hambly N. C., Dobbie P. D., Cross N. J. G., Christensen L., Martin E. L., Valdivielso L., 2011, *MNRAS*, 418, 2604
- Luhman K. L., 2004a, *ApJ*, 602, 816
- Luhman K. L., 2004b, *ApJ*, 617, 1216
- Mace G. N. et al., 2013, *ApJS*, 205, 6
- Makarov V. V., 2007, *ApJ*, 670, 1225
- Marley M. S., Saumon D., Cushing M., Ackerman A. S., Fortney J. J., Freedman R., 2012, *ApJ*, 754, 135
- Marsh K. A., Kirkpatrick J. D., Plavchan P., 2010a, *ApJ*, 709, L158
- Marsh K. A., Plavchan P., Kirkpatrick J. D., Lowrance P. J., Cutri R. M., Velusamy T., 2010b, *ApJ*, 719, 550
- Mužić K., Scholz A., Geers V., Jayawardhana R., Tamura M., 2012, *ApJ*, 744, 134
- Nakajima T., Oppenheimer B. R., Kulkarni S. R., Golimowski D. A., Matthews K., Durrance S. T., 1995, *Nature*, 378, 463
- Oppenheimer B. R. et al., 2013, *ApJ*, 768, 24
- Patten B. M. et al., 2006, *ApJ*, 651, 502
- Peña Ramírez K., Zapatero Osorio M. R., Béjar V. J. S., Rebolo R., Bihain G., 2011, *A&A*, 532, A42
- Peña Ramírez K., Béjar V. J. S., Zapatero Osorio M. R., Petr-Gotzens M. G., Martín E. L., 2012, *ApJ*, 754, 30
- Polletta M., Tajer M., Maraschi L., Trinchieri G., Lonsdale C. J., Chiappetti L., Andreon S., Pierre M., 2007, *ApJ*, 663, 81
- Rayner J. T., Toomey D. W., Onaka P. M., Denault A. J., Stahlberger W. E., Vacca W. D., Cushing M. C., Wang S., 2003, *PASP*, 115, 362
- Rebolo R., Zapatero Osorio M. R., Martín E. L., 1995, *Nature*, 377, 129
- Reylé C. et al., 2010, *A&A*, 522, 112
- Ridge N. A. et al., 2006, *AJ*, 131, 2921
- Roeser S., Demleitner M., Schilbach E., 2010, *AJ*, 139, 2440
- Rosenthal E. D., Gurwell M. A., Ho P. T. P., 1996, *Nature*, 384, 243
- Saumon D., Marley M. S., 2008, *ApJ*, 689, 1327
- Scholz A., Jayawardhana R., 2008, *ApJ*, 672, L49
- Scholz A., Muzic K., Geers V., Bonavita M., Jayawardhana R., Tamura M., 2012, *ApJ*, 744, 6
- Sheppard S. S., Cushing M. C., 2009, *AJ*, 137, 304
- Sorahana S., Yamamura I., 2012, *ApJ*, 760, 151
- Spezzi L., Alves de Oliveira C., Moraux E., Bouvier J., Winston E., Hudelot P., Bouy H., Cuillandre J.-C., 2012, *A&A*, 545, A105
- Tinney C. G., Burgasser A. J., Kirkpatrick J. D., McElwain M. W., 2005, *AJ*, 130, 2326
- Treister E. et al., 2006, *ApJ*, 640, 603
- Vacca W. D., Cushing M. C., Rayner J. T., 2003, *PASP*, 115, 389
- Wang W.-H., Cowie L. L., Barger A. J., Keenan R. C., Ting H.-C., 2010, *ApJS*, 187, 251
- Whitworth A., Bate M. R., Nordlund Å., Reipurth B., Zinnecker H., 2007, in Reipurth B., Jewitt D., Keil K., eds, *Protostars and Planets V*. Univ. Arizona Press, Tucson, AZ, p. 459
- Wilking B. A., Gagné M., Allen L. E., 2008, in Reipurth B., ed., *Handbook of Star Forming Regions, Volume II. The Southern Sky*, Astron. Soc. Pac., San Francisco, p. 351
- Zapatero Osorio M. R., Béjar V. J. S., Martín E. L., Rebolo R., Barrado y Navascués D., Mundt R., Eisloffel J., Caballero J. A., 2002, *ApJ*, 578, 536
- Zapatero Osorio M. R. et al., 2008, *A&A*, 477, 895

This paper has been typeset from a $\text{\TeX}/\text{\LaTeX}$ file prepared by the author.